NACA TN 4257

NATIONAL ADVISORY COMMITTEE FOR AERONAUTICS

TECHNICAL NOTE 4257

RESULTS OF AN EXPERIMENTAL INVESTIGATION OF SMALL VISCOUS DAMPERS

By Milton A. Silveira, Domenic J. Maglieri,
and George W. Brooks

Langley Aeronautical Laboratory
Langley Field, Va.

Washington
June 1958

1Q

NATIONAL ADVISORY COMMITTEE FOR AERONAUTICS

TECHNICAL NOTE 4257

RESULTS OF AN EXPERIMENTAL INVESTIGATION OF SMALL VISCOUS DAMPERS

By Milton A. Silveira, Domenic J. Maglieri, and George W. Brooks

SUMMARY

The results of an experimental investigation of several small viscous dampers are presented. The tests were made by means of a mechanical damper-test device, which facilitates testing of small dampers over a range of frequencies and amplitudes. The characteristics of the dampers are presented in the form of the magnitudes of the damping forces and spring forces as a function of the maximum velocity of the piston. Comparisons are made with data obtained from measurements of damping force by a beam damper-test device.

The damping characteristics of the dampers tested exhibited three general trends: (a) the damping force increased approximately linearly as the maximum piston velocity increased, (b) the damping force varied approximately as the square of the maximum piston velocity, and (c) the damping force varied approximately as the square root of the maximum piston velocity. The damping force and spring force measured for most dampers were found to be dependent on the maximum piston velocity and independent of frequency and amplitude other than for determining the piston velocity.

The test results showed, as expected, that temperature has a large effect on the force produced by the dampers and demonstrated the necessity for consideration of the heat generated and dissipated as a result of the work done by the damping force.

INTRODUCTION

The widespread use of dynamically scaled models for aeroelastic, dynamic, and aerodynamic studies has accentuated the need for information concerning the characteristics of various types of small dampers. Use of dampers on dynamic models is generally necessary either to simulate full-scale characteristics or to provide means of controlling the response of the model to applied forces or self-excited instabilities.

Familiar examples of damper installations are: drag-hinge dampers on rotor blades to control ground resonance, control-surface dampers on flaps, ailerons, and similar installations for flutter alleviation, and dampers for more general applications for shock relief. The lack of sufficient experimental data to aid in the selection of appropriate dampers for dynamic models that will provide the desired energy dissipation throughout the required operation range, yet will satisfy requirements for light weight, compactness, and reliability, is apparent. With the exception of reference 1, which presents results of an experimental and theoretical investigation of a small rotary shear damper, most of the available literature deals with large dampers not directly suitable for dynamic model applications.

In order to provide some information on dampers suitable for use on dynamic models, an investigation was made to determine the characteristics under different operating conditions of several types of small dampers which appeared promising. In recognition of the influence of fluid temperature and shear rate on the effective viscosity of prospective damper fluids, an attempt was made to investigate these effects on the characteristic behavior of the dampers.

A mechanical damper-test device was constructed to permit the frequency and amplitude to be varied conveniently over a wide range, and thus to obtain a variation in damper velocity either by variation of amplitude or frequency of damper motions. This device allows the total output force from the damper to be resolved into its damping and spring components and also permits the total force to be observed as a function of time.

The results of the damper studies together with a description of the damper-test devices are presented. A comparison of some simplified calculations with measured damping forces is also made.

SYMBOLS

a	decay coefficient, per sec
A	shear area, sq in.
c	clearance between piston and cylinder, in.
e_c	carrier voltage, volts
F	total force, lb

F_d	damping force, lb
F_s	spring force, lb
g_b	damping coefficient of beam
l	length of piston, in.
K,K_1,K_2,K_3	constants of calibration used for mechanical damper-test device
m_b	mass of beam, slugs
m_d	mass of damper, slugs
m_t	mass added to tip of beam, slugs
n	number of cycles
Δp	pressure change across piston, lb/sq in.
$h = \frac{c}{2}$	
r	radius of piston, in.
t,T	time, sec
v	velocity of fluid, in./sec
v_p	velocity of piston, in./sec
V	total volume of fluid, cu in.
V_d	total volume of fluid displaced, cu in.
x	amplitude of oscillation, in.
x_n	amplitude of nth oscillation, in.
y	increment from center line of clearance, in.
μ	absolute viscosity, lb-sec/sq in.
ω	circular frequency, radians/sec

ω_b natural frequency of beam, radians/sec

ω_d natural frequency of beam with damper attached, radians/sec

ω_c carrier frequency, radians/sec

DAMPER CONFIGURATIONS AND TEST APPARATUS

Description of Dampers

The damper configurations used in this investigation included six fluid-displacement dampers and four viscous-shear dampers. Schematic diagrams of the fluid-displacement dampers are shown in figure 1 and of the viscous-shear dampers, in figure 2. Fluids used in the dampers were commercially available petroleum oils with viscosities specified in Saybolt Universal seconds and silicone fluids with viscosities specified in centistokes. (For information on viscosity conversion, see ref. 2.)

Fluid-displacement single-chamber damper.- The dampers shown in figures 1(a), (b), and (c) consist of a piston moving through fluid contained within a cylinder. The dampers designated A-1 and A-2 were designed as aileron-flutter dampers, and seals between the piston shaft and the damper cylinder were omitted to minimize friction damping. An external pressurized oil source is utilized to replenish the fluid leakage past this clearance. Damper A-2 differs from damper A-1 in that the length of the piston is reduced, as shown in figure 1(b), to investigate the effect of physical modification of the piston.

Another single-chamber damper tested is damper B (fig. 1(c)), which is one of three drag dampers designed for a dynamic helicopter-rotor model. The piston of the damper contains two grooves running the length of the piston which can be altered to vary the damping force. The oil supply for this damper is maintained by gravity feed or centrifugal-pumping effects when installed on the rotor.

Fluid-displacement double-chamber damper.- The double-chamber dampers C and D shown in figures 1(d) and 1(e) permit a major portion of the fluid to bypass the piston by flowing through a secondary chamber. Since these dampers do not utilize seals between the piston shaft and the cylinder heads, an external pressurized oil source is necessary to eliminate the formation of air pockets within the damper. Damper D is a refinement of damper C in that the area of the slot between the chambers may

be varied. The area of the slot is adjusted by means of a worm screw which rotates the crescent-shaped liner of the secondary chamber.

Fluid-displacement bypass-tube damper.- Damper E, shown in figure 1(f), employs a bypass tube which contains a valve to restrict the flow of fluid through the tube. This damper employs "O" ring seals between the piston rod and damper body but, because of a small amount of leakage at the valve, an external pressurized oil source is used. Variation of the damping force is obtained by using the valve to restrict the flow and also by placing rods of 1-inch length and of various diameters in the part of the bypass tube parallel to the piston rod to reduce the cross-sectional area of the tube.

Viscous-shear neoprene-tube damper.- The viscous-shear neoprene-tube dampers are simple, lightweight dampers, which are easy to fabricate. This type of damper was specifically designed as a drag damper for a dynamic model helicopter rotor. Damper F, shown in figure 2(a), consists of a rod sliding through a section of neoprene tubing with silicone fluid used as the shearing fluid. The neoprene tubing is cemented to a section of steel tubing which is used in mounting the damper. Tests of damper F included variations in diameter of the damper rod of 0.178 and 0.180 inch. The neoprene tubing used was a standard commercially available tubing with nominal inside diameter of 0.1875 inch and a nominal outside diameter of 0.3125 inch.

A modification of damper F is damper G, which was designed to allow mechanical variation of the damping force. This damper, shown in figure 2(b), has the neoprene tubing moving with the piston rod, which slides through the brass sleeve. The force output of the damper is increased by placing rings to compress the length of the neoprene piston, which thus increases the piston diameter.

A further modification of damper F is damper H shown in figure 2(c). In order to provide a supply of fluid for extensive operation, two sections of neoprene tubing are cemented at some distance apart inside a length of metal tubing to form a chamber for the fluid.

Viscous-shear metal damper.- Shown in figure 2(d) is a viscous-shear damper fabricated from aluminum. Unlike the neoprene-tube dampers, the clearance between the piston rod and cylinder of the all-metal damper can readily be determined. A high-viscosity (70,000 centistokes) silicone fluid was used as the shearing fluid in this damper.

Test Devices

The general characteristics of the dampers were obtained by means of a mechanical damper-test device designed and constructed for such

investigations. Some tests were also made by attaching dampers to the end of simple cantilever beams in order to obtain a comparison of the results by the two methods. The details of the two test devices are presented in the following sections.

Mechanical damper-test device.- The mechanical damper-test device shown in figures 3 and 4 affords a means of conveniently varying the frequency and amplitude of the reciprocating motion applied to the damper. The test device is driven at rotational speeds of from 100 to 3,000 rpm by a water-cooled electric motor possessing a relatively large inertia and large power capacity to insure that a constant frequency is maintained whenever a load is suddenly applied to the system. The rotational motion of the electric motor is converted to a reciprocating motion (see fig. 4) by use of an eccentric drive and a slide block contained within the amplitude arm. The amplitude arm moves in an arc with the center of motion located on the track of the amplitude arm. The connecting rod is attached to the amplitude arm and drive rod by pin joints. This connection results in a reciprocating motion of the drive rod. Variation of the amplitude of the displacement of the damper is effected by the movement of the amplitude arm through an azimuth of 90°, and this motion in turn positions the slide block. When the amplitude arm is in the vertical position, the amplitude of the motion imparted to the damper is that of the eccentric, but when this arm is in the horizontal position the slide block moves within the amplitude arm, and very little motion of the damper results. Intermediate positions of the amplitude arm provide an additional selection of the amplitude of motion without necessitating a change of eccentrics. Eccentricities of ±1/8 inch, ±1/4 inch, and ±3/8 inch were used for the tests.

In order to insure that the motion of the damper very closely follows that of a sine wave for small displacements, it is necessary to minimize all clearances of the bearings, slide block, and pin joints. A journal bearing is used between the eccentric and the slide block. Because of these small clearances, an air-mist lubrication system utilizing an extreme-pressure lubricant is used on the slide block and eccentric bearing.

The damper piston rod is attached to the drive system by means of pin joints to insure that no side loads can be transmitted to the damper piston. The body of the damper is fixed to the load cell, which is used to measure the forces transmitted by the damper. The load cell had a natural frequency of approximately 1,500 cps and a deflection at maximum load of 0.0015 inch. This high spring rate, in conjunction with the small inertia of the damper body, resulted in negligible magnification of the damper force put out by the load cell.

A detailed discussion of the instrumentation used to separate the forces transmitted by the damper into components in phase and out of phase with the displacement is presented in appendix A.

Beam damper-test device.- The device used to obtain the characteristics of a damper by use of a deflected beam is shown in figure 5. The damper piston is attached to the tip of a cantilever beam by means of a pin-joint arrangement, and the damper cylinder is attached to the load cell. The beam is then deflected initially to the desired amplitude and suddenly released, so that a logarithmic oscillation is produced. A strain gage mounted at the root of the beam was calibrated to measure the static deflection at the beam tip. The desired beam frequencies were established by attaching appropriate additional masses to the tip. Inasmuch as the piston displacement is measured by using the beam-displacement strain gage, it is of utmost importance that freedom in the pin joint be held to a minimum and that the root of the cantilever beam be rigid in order to assure that the beam and piston displacements are identical. In this investigation, a differential transformer was placed at the tip of the beam to measure the actual beam tip deflection during the tests. The tip deflections obtained from the strain gages mounted at the beam root compared very well with the results obtained from the differential transformer mounted at the beam tip.

The beam damper-test device gives the characteristics of the damper by means of the logarithmic decrement of the decay of the oscillation as indicated by strain gages mounted on the beam, while at the same time the total force output of the damper is being measured by the load cell.

METHOD OF TESTS

Method Used With Mechanical Damper-Test Device

In tests of the dampers by means of the mechanical damper-test device, the amplitude arm is initially maintained in the horizontal position until the desired frequency is obtained. Once the desired frequency is reached, the amplitude arm is quickly placed at the desired displacement setting. This procedure is used to avoid premature heating of the damper and also to permit time-history studies of the damper characteristics at a given frequency. Because of initial fluctuations of the averaging meter, approximately 10 seconds elapsed before each of the two force values could be read. If heating of the damper was excessive, the damper was cooled to the initial temperature before being tested at another frequency or amplitude. Each damper was tested at several frequencies and amplitudes.

For specific tests designed to determine the effects of temperature on the variation of the force output of the damper, elimination of the usual instrumentation was necessary because of the time interval required before the force could be read. The force output of the damper, measured by the load cell, was then recorded directly on an oscillograph and the

temperature of the damper, as indicated by a thermocouple mounted on the outside of the cylinder, was read at the same time interval. Inasmuch as the resolver circuit was not included in recording the load-cell signal, separation of the damping and spring forces was not possible.

Method Used With Beam Test Apparatus

In tests with the damper attached to the tip of a cantilever beam, the beam is initially deflected to the desired amplitude and suddenly released, so that a decaying oscillation is produced. The decrement of the beam oscillation measured by the beam strain gage and the response of the load cell are recorded simultaneously on oscillograph records.

The damping force is then obtained from the logarithmic decrement of the decay of the oscillation by a method similar to that described in reference 3 and is given by

$$F_d \approx \left[-2a\omega_d\left(\frac{1}{4} m_b + m_t + m_d\right) - g_b\omega_b^2\left(\frac{1}{4} m_b + m_t\right)\right]\frac{x}{12} \tag{1}$$

where

$$a = -\frac{\omega_d}{2\pi n} \log_e \frac{x}{x_n} \tag{2}$$

The results obtained by the beam damper-test device were also used as a check on the calibration of the mechanical damper-test device. This check was accomplished by measuring the damping force of a damper similar to damper A-2 having a very low spring force with the mechanical damper-test device and comparing these values with those obtained by measurements of the same damper with the beam damper-test device. This comparison, shown in figure 6, indicates good agreement between the results obtained by the two methods.

RESULTS AND DISCUSSION

The characteristic measured force-velocity curves of the dampers studied are first discussed. The effects of changing the force characteristics of some of the dampers by varying their fluid properties or geometry are then experimentally evaluated. Particular attention is given to the significant effects of temperature exhibited by the dampers investigated. Finally, the measured force results are compared with some simple calculations for both fluid-displacement and viscous-shear dampers.

General Characteristics

The characteristic curves for each damper were derived by measuring the maximum damping and spring forces developed during the cycle for several frequencies and amplitudes with the mechanical damper-test device. These data are presented in figures 7 to 19 as curves of force plotted against the maximum velocity of the piston during a cycle.

The damping-force data exhibited three general trends which are illustrated by the data of figures 7, 8, and 9. The first of these trends is shown in figure 7, where results for damper A-2 show that the damping force varies approximately linearly with the velocity. Furthermore, the data were measured at various frequencies and amplitudes. The results for this damper and all other dampers tested, with one exception to be discussed separately, indicate that the force is dependent upon only the velocity of the piston, within the range of these tests. This type of damper thus provides a damping coefficient (force divided by velocity) that is constant throughout the range of velocities. This linear trend of damping force is also exhibited by dampers having widely different physical arrangements as illustrated by the data for dampers B and E in figures 10 and 16.

The second trend is shown in figure 8 for damper C, and little damping is found to be provided at low maximum piston velocities, but as the piston velocity increases, the damping force increases approximately as the square of the piston velocity.

The third trend is illustrated by the data in figure 9 for damper A-1, which shows that the damping force varies approximately as the square root of the piston velocity. This last trend is also exhibited by dampers F-1, F-2, G, H, and J. (See figs. 11, 12, 13, 14, and 19.)

Variation of Damping Force

During tests to measure the force-velocity relationship of the dampers, the opportunity was taken to evaluate the amount of variation of the damping force obtainable by some alteration of the damper physical properties. These later alterations pertained to such parameters as fluid viscosity, piston shape, clearance, and fluid valving. These results are considered of practical significance with regard to specific applications in dynamic model work.

Fluid properties.- Each fluid-displacement damper with an external pressurized oil source was tested with an oil having a viscosity of 300 Saybolt Universal seconds at 100° F. Variation of the pressure between 10 and 60 pounds per square inch had little effect on the damping force. Damper B, which used a gravity-feed fluid-supply system, was

tested with silicone fluid having a viscosity of 50 and 100 centistokes at 77° F. The curves presented in figure 10 show that the variation of damping force of this damper with maximum piston velocity is approximately linear. Comparison of the curves for the 100-centistoke silicone fluid and the 50-centistoke silicone fluid indicates that the measured damping force is not quite doubled. This characteristic would indicate either a change of the flow within the damper or a change in the apparent viscosity of the fluid.

The shear dampers tested employed silicone fluids having viscosities of 3,000, 20,000, and 70,000 centistokes at 77° F. High-viscosity silicone fluids exhibit the property of pseudoplastic flow; that is, the fluid is essentially non-Newtonian (the dynamic viscosity decreases as the shear rate is increased) in behavior at high shear rates. The apparent change in viscosity with shear rate can be seen in figure 20, which data are taken from reference 4. Judging from the change shown, as the shear rate increases, the damping force measured would vary approximately as the square root of the velocity because of the existence of thixotropy (a gel becoming a fluid when shaken). Such a trend was exhibited by all of the viscous shear dampers at the high shear rates.

The general characteristics of the viscous shear damper F-1 measured for viscosities of 20,000 and 70,000 centistokes are shown in figure 11. Because of the uncertainty of the clearance between the piston rod and the neoprene tubing throughout the length of the damper, the shear rate can only be estimated. A conservative estimate would encompass shear rates (piston velocity divided by the clearance) in excess of 100 reciprocal seconds. The shear rates are, however, within the non-Newtonian behavior range of the fluid for all maximum piston velocities except extremely low values of 0.1 or 0.2 inch per second or lower.

In order to determine the clearance between the shearing areas more readily, an all-metal shear damper J was tested, and these results are shown in figure 12. The shear rate for a maximum piston velocity of 1 inch per second is 1,000 seconds^{-1}, which is well within the non-Newtonian range for the 70,000-centistoke silicone fluid used in the damper. As shown in figure 20, which is taken from reference 4, the apparent viscosity of the 70,000-centistoke silicone fluid is approximately 25,000 centistokes for a shear rate of 1,000 seconds^{-1}. For a piston velocity of 10 inches per second the apparent viscosity of the fluid is one-tenth of the initial viscosity or 7,000 centistokes.

In order to determine whether any marked change in the general characteristic of a viscous-shear damper would result from a reduction of the piston-rod diameter and a corresponding subsequent reduction in shear rate for the same piston-rod velocity, damper F-2 was tested, and the results are compared with those of damper F-1 in figure 13. The

magnitude of the data was altered but the characteristic shape of the curve remained the same.

Damper H was tested to determine whether the general characteristics of a viscous-shear damper would change from the characteristics shown by damper F-1 when the sections of neoprene tubing were divided and fluid was placed between them. The results are shown in figure 14. Again there was a change in magnitude, as would be expected, due to an increase in piston-rod diameter to 0.183 inch but the general characteristics of the curve remained the same.

Damper geometry.- Tests were performed on three dampers that incorporated provisions in their design allowing variation of the geometry which would result in a variation of the damping force. Damper D (fig. 1(e)), a refinement of the double-chamber type of damper, contains provisions for variation of the area of the slot between the primary and secondary chambers. Figure 15 presents the variation of damping force that can be obtained by varying the slot from maximum to minimum opening. If the area of the slot is maintained at some intermediate value as the velocity is increased, the damping-force curve will maintain approximately the same shape as those for the limiting values shown in this figure. This damper produced no spring force for the range of amplitude and frequency of the tests.

Another variable-geometry damper investigated was damper E but, unlike other dampers used in this investigation, the damping force and spring force produced by damper E were dependent upon both the frequency and amplitude of the oscillation and not on the piston velocity alone, as is shown in figure 16 for the condition with the bypass valve partly closed. Inasmuch as a force of 0.85 pound is required to move the piston because of the piston-rod "O" ring seal, the curves should originate from this value of force at zero piston velocity. The force required to move the piston once the motion is started was found to be less than this breakout force, as can be seen from the figure.

The characteristics of damper E were studied, as follows: First, the damper was tested at three different amplitudes with partial constriction in the bypass tube obtained by positioning a screw mounted so as to enter the tube at right angles. The results of these tests are given in figure 16, where the curves indicate approximately linear damping- and spring-force characteristics. The results also indicate that at a given velocity, the damper forces are proportional to the displacement and that this damper is characterized by large spring forces.

Subsequent to the aforementioned tests, tests were made at a constant amplitude of 0.123 inch to determine the effects of variations of the constrictions in the bypass tube. The constrictions were varied both by adjusting the screw entering the bypass tube and by inserting

rods of different diameter in the bypass tube. The results of these studies are given in figures 17 and 18. Figure 18 shows that constrictions of the area of the bypass tube of the order of 25 percent or less had little effect on the damping force. A similar result was also observed when the area was varied by adjusting the screw.

The possible range of damping available by using compression rings (washers) to compress the length and thus increase the diameter of a neoprene piston of a viscous-shear damper is presented for damper G in figure 19. As compression is increased by adding these spacers, the damping obtained will vary from viscous damping with little friction damping to pure friction damping. The upper limit presented, which was considered mostly friction damping, resulted from compressing the piston length 0.08 inch. This amount of compression increased the unrestricted piston diameter of 0.315 inch. The inside diameter of the cylinder was 0.313 inch.

Of interest is a comparison of the results of measured damping force of dampers A-1 and A-2 presented in figures 7 and 9. These dampers differ only in the shape of the piston. The cylindrical piston of damper A-1 (fig. 1(a)) was modified to the shape shown in figure 1(b) and designated damper A-2. The modification resulted in a marked reduction in damping force, and the damping force became an approximately linear function of velocity. Also of interest is the elimination of the spring force.

Effects of Temperature

The effect of temperature on the damping force was investigated to determine the manner and extent to which the general characteristics of the dampers are affected. The variation of the viscosity with temperature for the fluids used in the dampers of this investigation is shown in figure 21, which has been prepared in conformity with the standards of the American Society for Testing Materials.

Inasmuch as approximately 10 seconds elapsed before the force values obtained with the mechanical damper-test devices could be read, a considerable reduction in the damping force could result at the higher piston velocities by using the mechanical damper-test device. In order to investigate the effect of temperature on the damping force, the 10-second time lapse prior to reading the force had to be avoided. This was accomplished by recording the output of the load cell directly on an oscillograph recorder. Since the load cell measures the total damping force, a damper similar to damper A-2, which develops very little spring force was used. Figure 22 illustrates the change in damping force with time caused by the conversion of work into heat, which thus reduces the apparent viscosity of the fluid. A substantial reduction of the damping force

occurs during the initial 30 seconds of operation but as the heat generated becomes equal to that dissipated, the damping force also reaches a constant level. Since the thermocouple is located on the exterior of the damper chamber, the actual temperature in the chamber probably stabilizes sooner than shown. Two amplitudes are shown for the same frequency and the resultant differences in rate of heating and loss of damping force can be seen.

The results obtained on the mechanical damper-test device, shown in figures 7 to 19, were obtained approximately 10 seconds after the initial forced oscillation. Therefore the damping force measured at the higher piston velocities is somewhat lower than the initial force output. For the range of amplitudes and frequencies used during the damper tests, it was determined that the characteristic trends of the force-velocity curves are not altered by temperature.

The effect of temperature on small model dampers requires consideration of the application of the damper in the determination of the damping force. If the damper is to be used in a model control system to prevent flutter, the initial damping force would probably be of primary concern. If the application of the damper requires continuous operation, as in the case of a helicopter drag damper, the value of the force after the temperature stabilizes would probably be appropriate.

Comparison With Theory

The damping force for a damper similar to damper A-2 was calculated by using the formula

$$\frac{F_d}{v_p} = 6\pi\mu l\left(\frac{r}{c}\right)^3 \tag{3}$$

which is derived in the appendix B. In this equation, F_d is the damping force, v_p is the piston velocity, μ is the absolute viscosity, l is the length of the piston, r the radius of the piston, and c the clearance between piston and cylinder. This method considered the displacement of fluid only and is used to obtain an approximate value of the damping force. Figure 23 compares the results for a damper similar to damper A-2 obtained on the beam damper-test device (fig. 5) with calculated values. The calculated values are somewhat higher than the measured values, as would be expected, because consideration has not been given to the fluid volume lost in passing the piston rod, in addition to the fact that the flow is assumed to be ideal.

Inasmuch as the damping-force values presented in figure 23 were measured by the beam method, it is also assumed that the viscosity of

the fluid was not affected by temperature; however, the possibility exists that a small area such as that around the piston may generate temperatures affecting the viscosity and flow of the fluid in that area.

The calculations for viscous-shear damper J shown in figure 24 were made by using the formula

$$\frac{F_d}{v_p} = \mu\left(\frac{A}{c}\right) \tag{4}$$

Where A is the shear area and where the absolute viscosity is corrected to consider the non-Newtonian characteristics of the fluid presented in figure 20. The calculated values of the damping force are much greater than those measured on the mechanical damper-test device as indicated by the top dashed curve of figure 24. However, if consideration is given to the decrease in viscosity due to the temperature generated, as indicated by the curves of figure 21, fair agreement can be expected as shown by the lower dashed curve of figure 24. The points on the lower curve were calculated on the assumption that all heat generated by the damper, in the 10-second interval required before a reading was obtained, remained in the fluid. This assumption is not valid when the temperature gradient increases with high shear rates, as indicated by the reduction of the calculated forces at the higher velocities, and hence it appears that the heat transferred to the damper body must be considered in determining the temperatures and viscosity of the fluid.

CONCLUDING REMARKS

Results are presented for a number of different designs of small fluid-displacement or viscous-shear dampers suitable for dynamic model application and the characteristic behavior of the damping forces are shown as a function of damper velocities. The damping-force—velocity relationships were found to exhibit three general trends as follows:
(a) the damping force varies approximately linearly with velocity;
(b) the damping force varies approximately as the velocity squared; and
(c) the damping force varies approximately as the square root of the velocity.

The damping force and spring force measured for all dampers except one were independent of frequency and amplitude except for the effect of frequency and amplitude in determining the maximum piston velocity throughout the range of the tests.

As a result of the non-Newtonian characteristic of silicone fluids, the damping force of the viscous-shear dampers tested increases at a smaller rate as the shearing rate is increased.

The heat generated by a small viscous damper has a great effect on the damping force produced. Consideration must be given to the application of the damper and the effect of temperature to obtain the damping force required.

A simplified calculation presented indicates that temperature effect must be considered in the determination of the damping force. Calculation of the damping force of a fluid-displacement damper requires consideration of the type of fluid flow in the damper, whether it be laminar or turbulent, and the amount of leakage of fluid past the piston shaft in addition to the effect of temperature.

Langley Aeronautical Laboratory,
National Advisory Committee for Aeronautics,
Langley Field, Va., March 3, 1958.

APPENDIX A

MECHANICAL DAMPER-TEST-DEVICE INSTRUMENTATION

The damper force is resolved into the component in phase with the damper displacement and the component in phase with the damper velocity by means of a resolver, by a technique similar to that described in reference 5. The resolver is a precision-wound transformer with two secondary windings on a rotor. These two windings are spaced at 90° on the rotor, so that as the rotor turns through an angle ωt, one winding multiplies the transformation ratio by $\cos(\omega t)$, and the other winding multiplies it by $\sin(\omega t)$. Thus, if a carrier signal is applied to the primary of the resolver, as shown in the block diagram of figure 25, the output voltages from the secondary windings are

$$e_c \sin(\omega_c t)\sin(\omega t)$$

$$e_c \sin(\omega_c t)\cos(\omega t)$$

The drive-motor shaft is coupled directly to the resolver rotor and also to the damper through an eccentric, which converts the rotary motion into a sinusoidal, translational motion. If the resolver stator is positioned relative to the rotor, the output voltages of the resolver may be adjusted accurately in phase with the damper velocity and damper position. These resolver output voltages are applied, one at a time, through an amplifier of gain K to the load-cell strain-gage bridge. The output of this bridge is proportional to the product of the damper force and the modulated carrier signal.

The total force is

$$F(t) = F_s \sin(\omega t) + F_d \cos(\omega t)$$

This force appears on the strain-gage bridge as

$$K_2\left[F_s \sin(\omega t) + F_d \cos(\omega t)\right]$$

The product of this quantity and the amplified carrier signal with the resolver switch in one position is equal to

$$K_1\left[F_s \sin(\omega t) + F_d \cos(\omega t)\right] K_2\left[e_c \sin(\omega_c t)\sin(\omega t)\right]$$

or

$$K_1K_2e_c \sin(\omega_c t)\left[F_s \sin^2(\omega t) + F_d \sin(\omega t)\cos(\omega t)\right]$$

and with the resolver switch in the other position

$$K_1\left[F_s \sin(\omega t) + F_d \cos(\omega t)\right]K_2\left[e_c \sin(\omega_c t)\cos(\omega t)\right]$$

or

$$K_1K_2e_c \sin(\omega_c t)\left[F_s \sin(\omega t)\cos(\omega t) + F_d \cos^2(\omega t)\right]$$

These unbalance outputs are again amplified (K_3) and passed through a phase-sensitive demodulator, which merely removes the carrier frequency (ω_c). The result is then read on an averaging meter. Since

$$\lim_{T \to \infty} \frac{1}{T} \int_0^T \sin(\omega t)\cos(\omega t)dt = 0$$

and

$$\lim_{T \to \infty} \frac{1}{T} \int_0^T \sin^2(\omega t)dt = \lim_{T \to \infty} \frac{1}{T} \int_0^T \cos^2(\omega t)dt = \frac{1}{2}$$

the voltage read on the averaging meter with the switch in one position is

$$\frac{1}{2} K_1K_2K_3F_s$$

or with the switch in the other position

$$\frac{1}{2} K_1K_2K_3F_d$$

The constants K_1, K_2, and K_3 may be evaluated statically from a calibration. Thus, the real or spring-force component F_s and the imaginary or damping-force component F_d of the total force may be read directly.

One of the merits of this technique is that higher harmonics (or noise) have a small effect on the results, since

$$\lim_{T \to \infty} \frac{1}{T} \int_0^T \sin(\omega t)\sin(nt)dt = 0$$

as long as $n \neq \omega$ and thus

$$\lim_{T \to \infty} \frac{1}{T} \int_0^T \sin(\omega t)F(t)dt = 0$$

if $F(t)$ has no component which is correlated with $\sin(\omega t)$.

At very low operating frequencies of the drive system, the averaging meter used has a tendency to follow the alternating-voltage component unless the meter is excessively damped. Therefore, the instrumentation prohibits testing of dampers at frequencies below about 1.5 cps.

APPENDIX B

CALCULATION OF DAMPING FORCE

A simplified method of determining the damping force that can be used for a damper which obtains the damping force due to fluid displaced rather than to the shearing of the fluid is presented as a possible guide to use in designing a fluid-displacement damper. For the present purpose, consider the configuration shown in the following sketch:

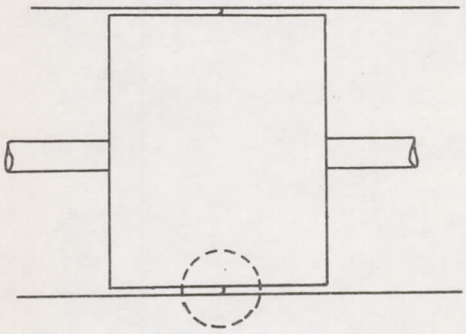

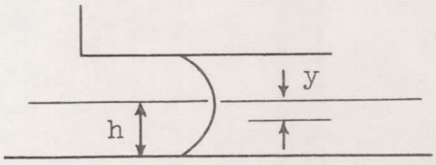

Enlarged view of dotted area

The velocity gradient between the piston and cylinder shown in this sketch can be written as

$$\frac{dv}{dy} = \frac{\Delta p(h - y)}{\mu l}$$

Integrating this expression gives the velocity, as follows:

$$v = \frac{\Delta p}{\mu l}\left(hy - \frac{y^2}{2}\right)$$

The total volume of flow is

$$V = 2\pi r \int_{-h}^{h} v \, dy$$

Integrating and writing in terms of the clearance gives

$$V = \frac{\pi}{6} \frac{\Delta p}{\mu l} c^3 r$$

The total volume displaced in terms of the velocity of the piston is

$$V_d = v_p \pi r^2$$

and

$$v_p = \frac{1}{6} \frac{\Delta p}{\mu l} \frac{c^3}{r}$$

The ratio of the force to piston velocity is therefore

$$\frac{F_d}{v_p} = 6\pi\mu l \left(\frac{r}{c}\right)^3$$

REFERENCES

1. Lees, Sidney: Investigation of the Performance of an Experimental Viscous Shear Type Damper. MIT Rep. 6398-T-5, 1948.

2. Marks, Lionel S., ed.: Mechanical Engineers' Handbook. Fifth ed., McGraw-Hill Book Co., Inc., 1951, pp. 230-232.

3. Scanlan, R. H., and Rosenbaum, R.: Introduction to the Study of Aircraft Vibration and Flutter. The Macmillan Co., 1951, p. 68.

4. Currie, C. C., and Smith, B. F.: Flow Characteristics of Organopolysiloxane Fluids and Greases. Ind. and Eng. Chem., vol. 42, Dec. 1950, pp. 2457-2462.

5. Queijo, M. J., Fletcher, Herman S., Marple, C. G., and Hughes, F. M.: Preliminary Measurements of the Aerodynamic Yawing Derivatives of a Triangular, a Swept, and an Unswept Wing Performing Pure Yawing Oscillations, With a Description of the Instrumentation Employed. NACA RM L55L14, 1956.

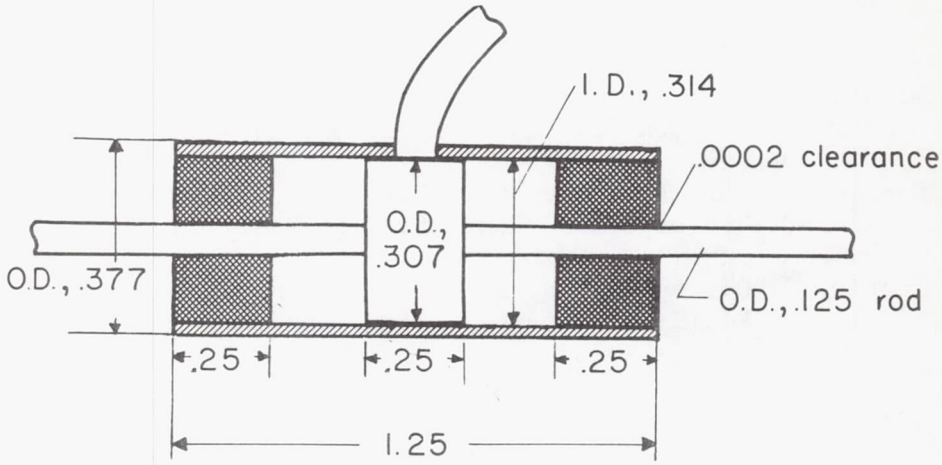

(a) Damper A-1.

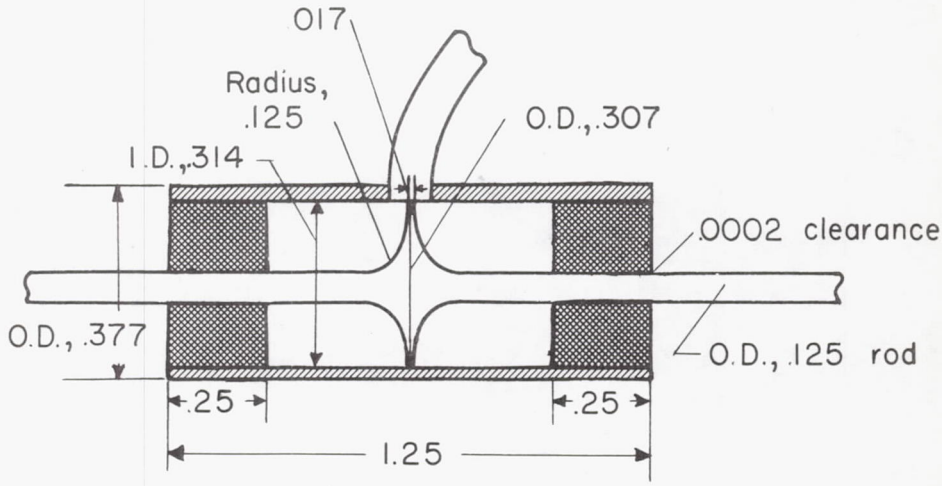

(b) Damper A-2.

Figure 1.- Fluid-displacement dampers. (All dimensions in inches.)

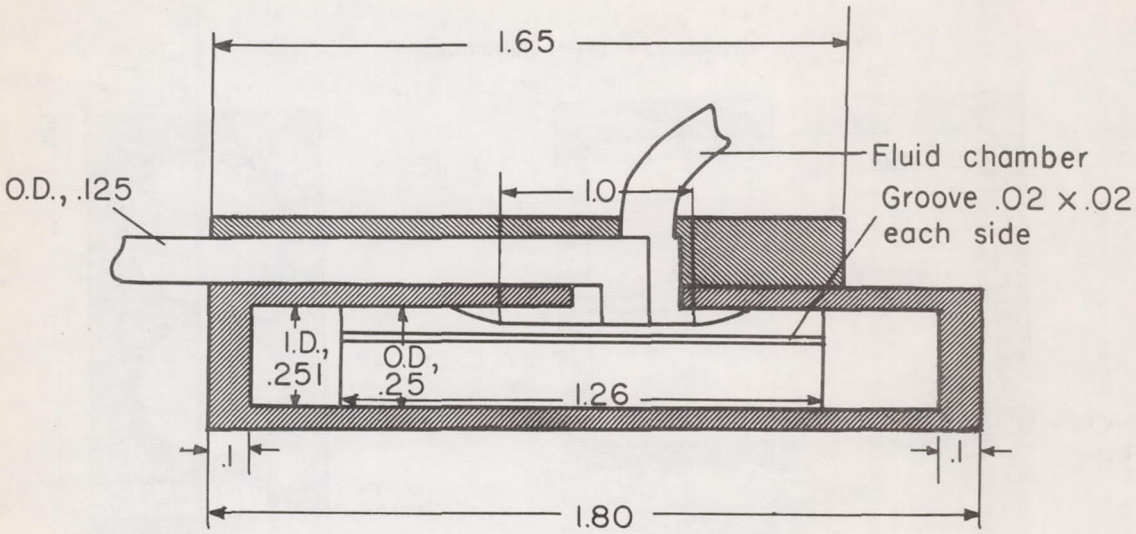

(c) Damper B.

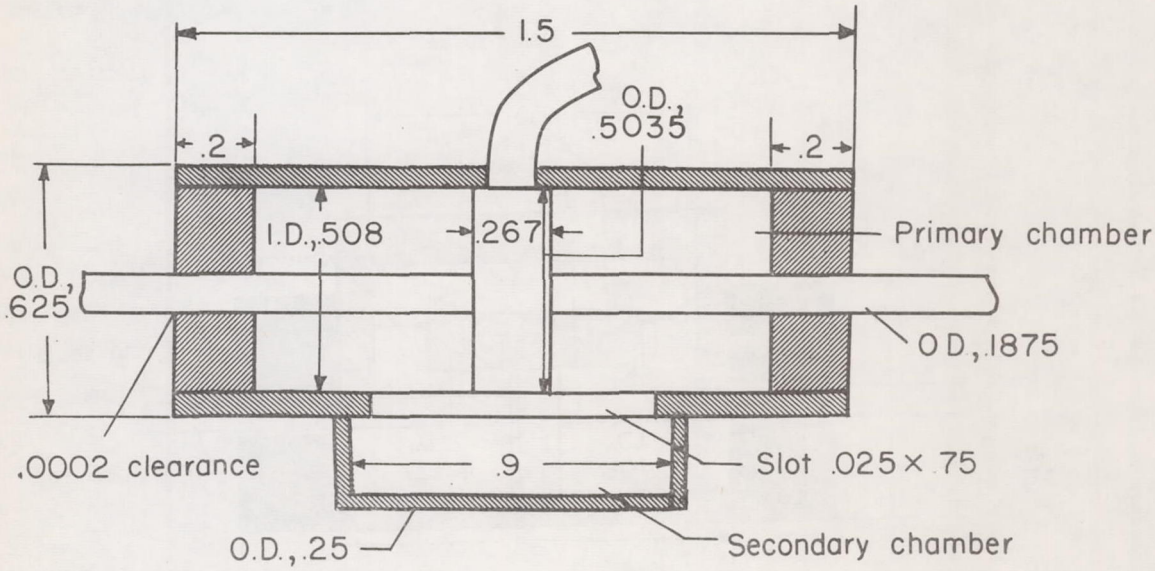

(d) Damper C.

Figure 1.- Continued.

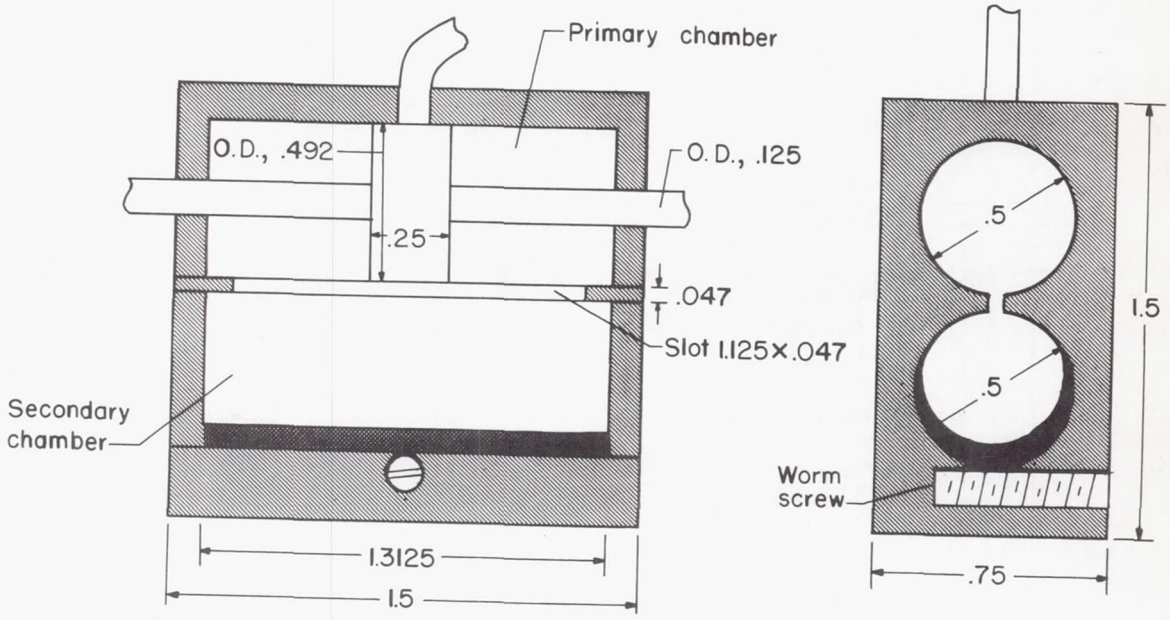

(e) Damper D.

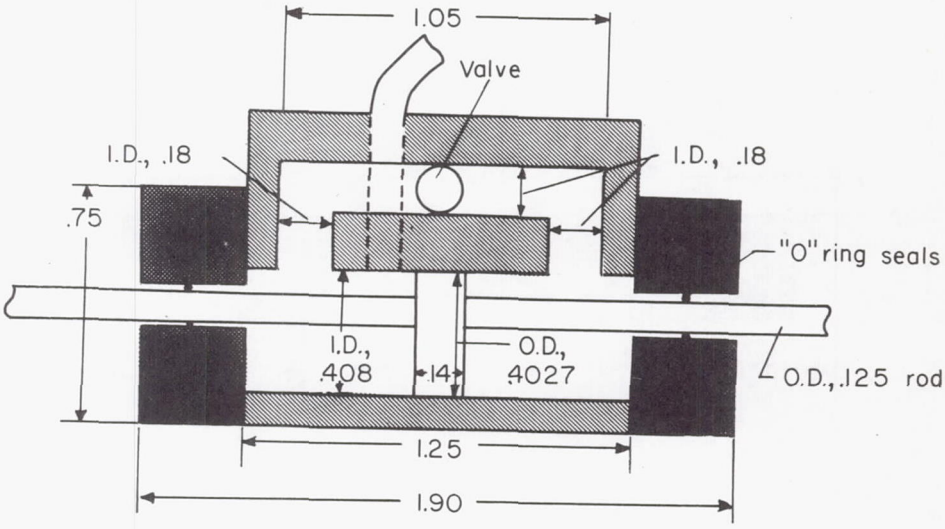

(f) Damper E.

Figure 1.- Concluded.

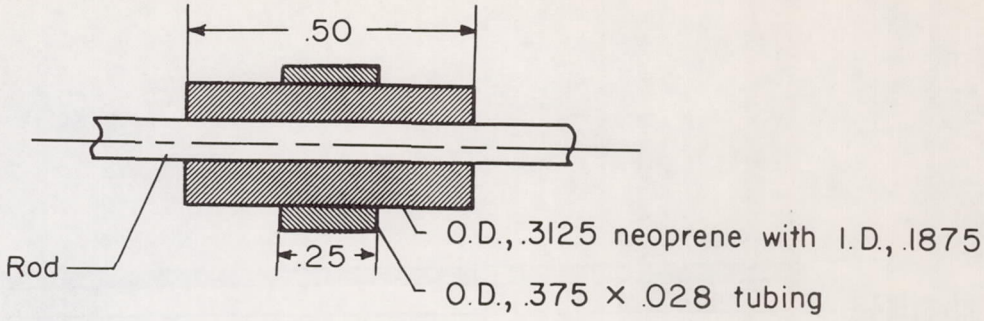

Damper	Rod diam.
F-1	.180
F-2	.178

(a) Damper F.

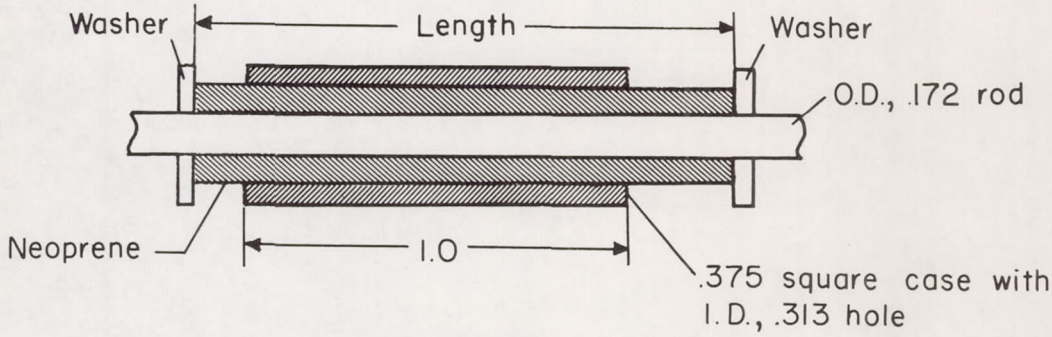

Spacers	Neoprene O.D.	Neoprene length
0	.305	1.40
All	.315	1.32

(b) Damper G.

Figure 2.- Viscous-shear dampers. (All dimensions in inches.)

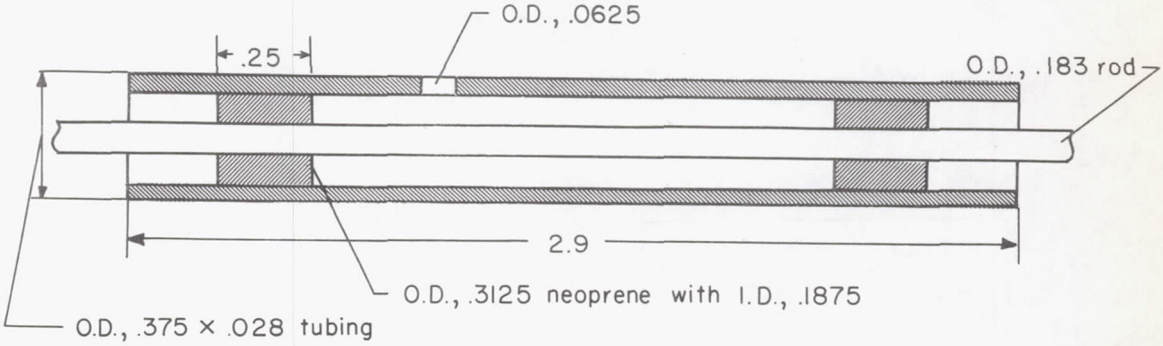

(c) Damper H.

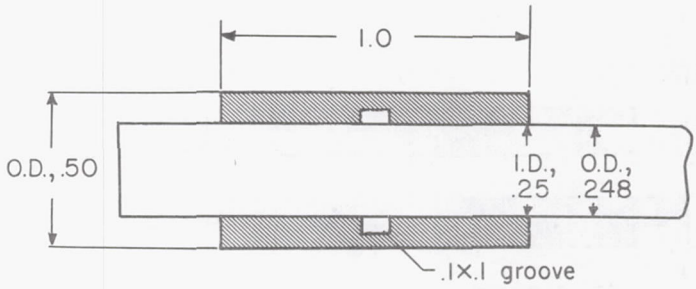

(d) Damper J.

Figure 2.- Concluded.

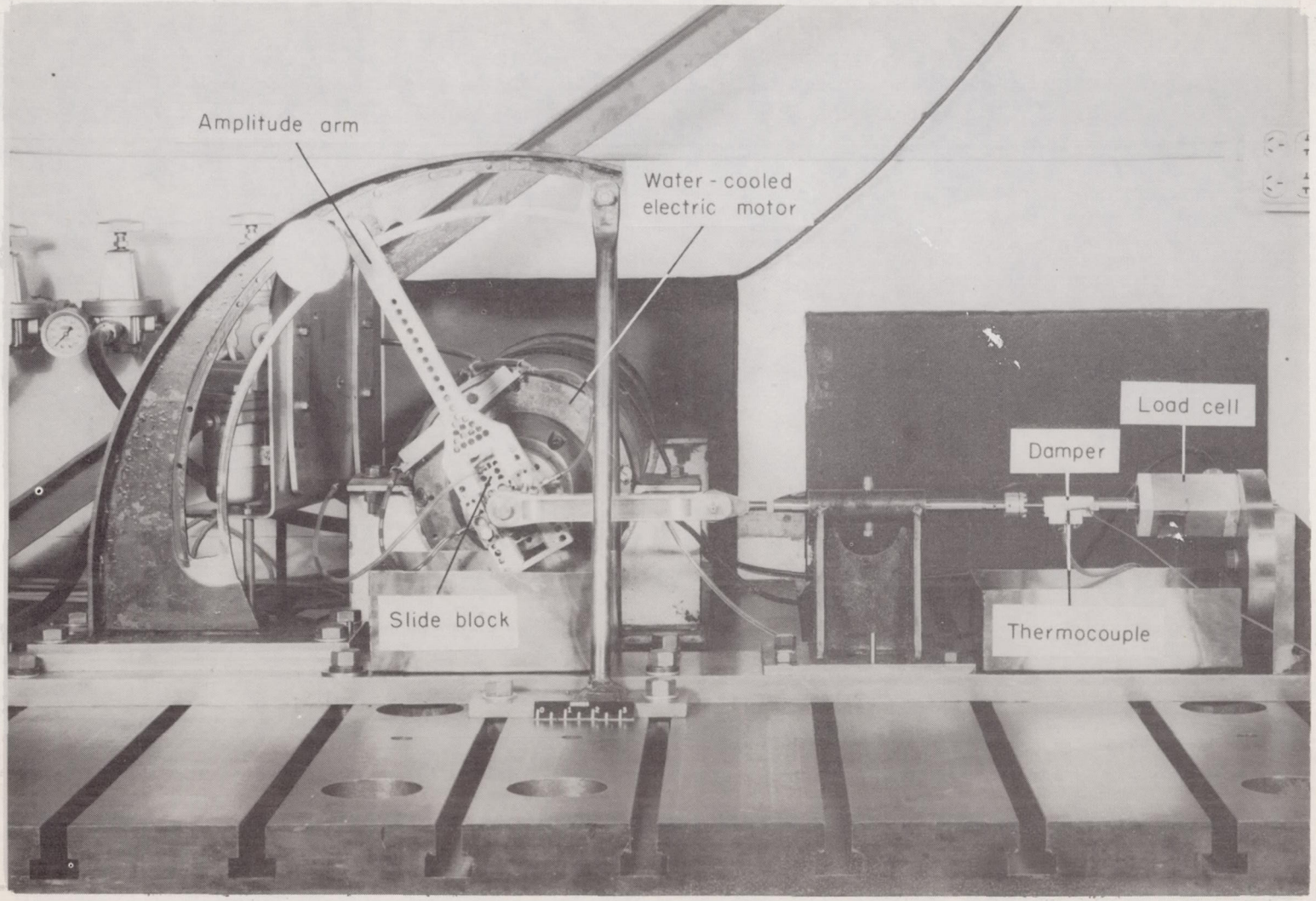

Figure 3.- Mechanical damper-test device. L-57-1414.1

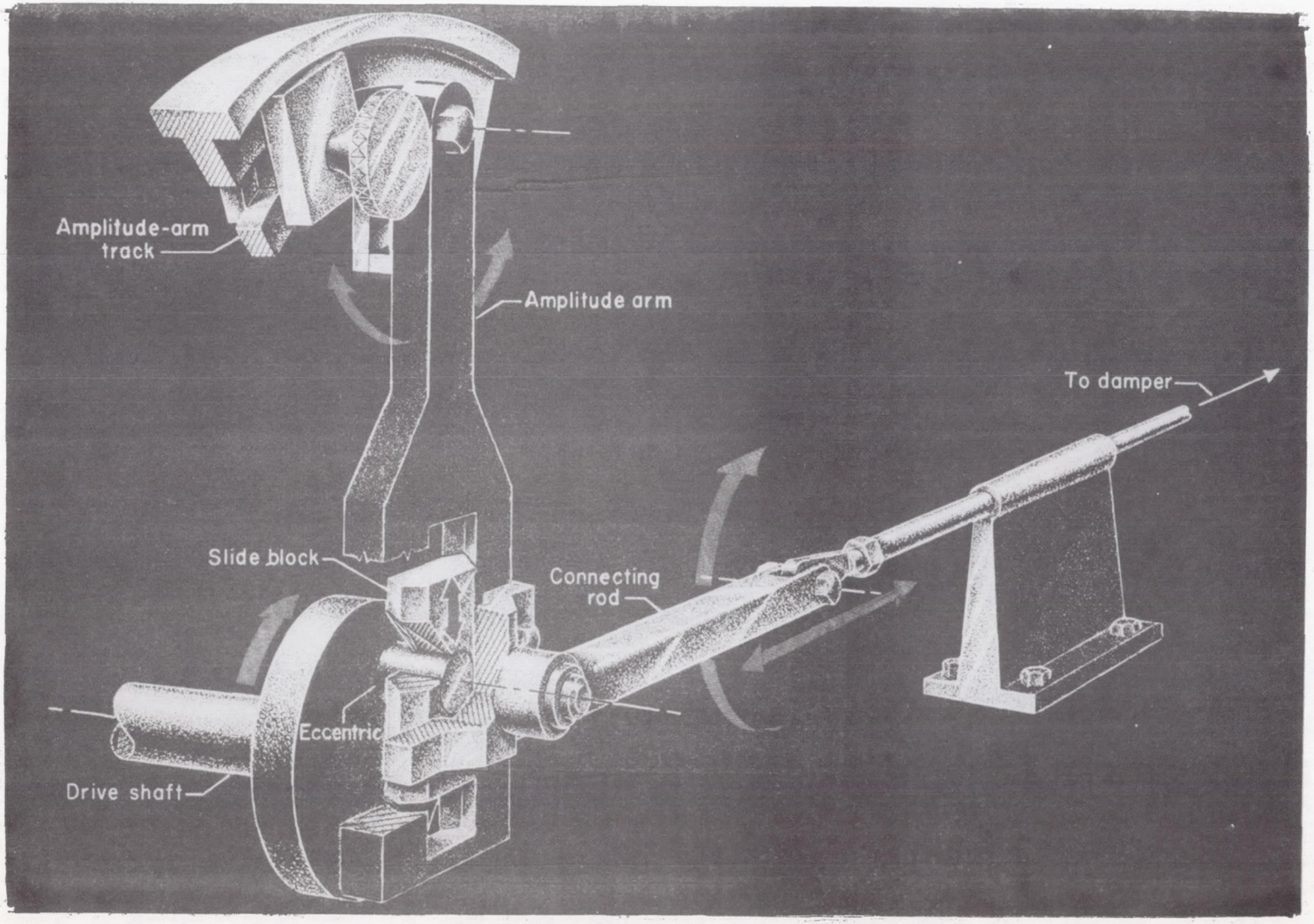

Figure 4.- Drive system of mechanical damper-test device.

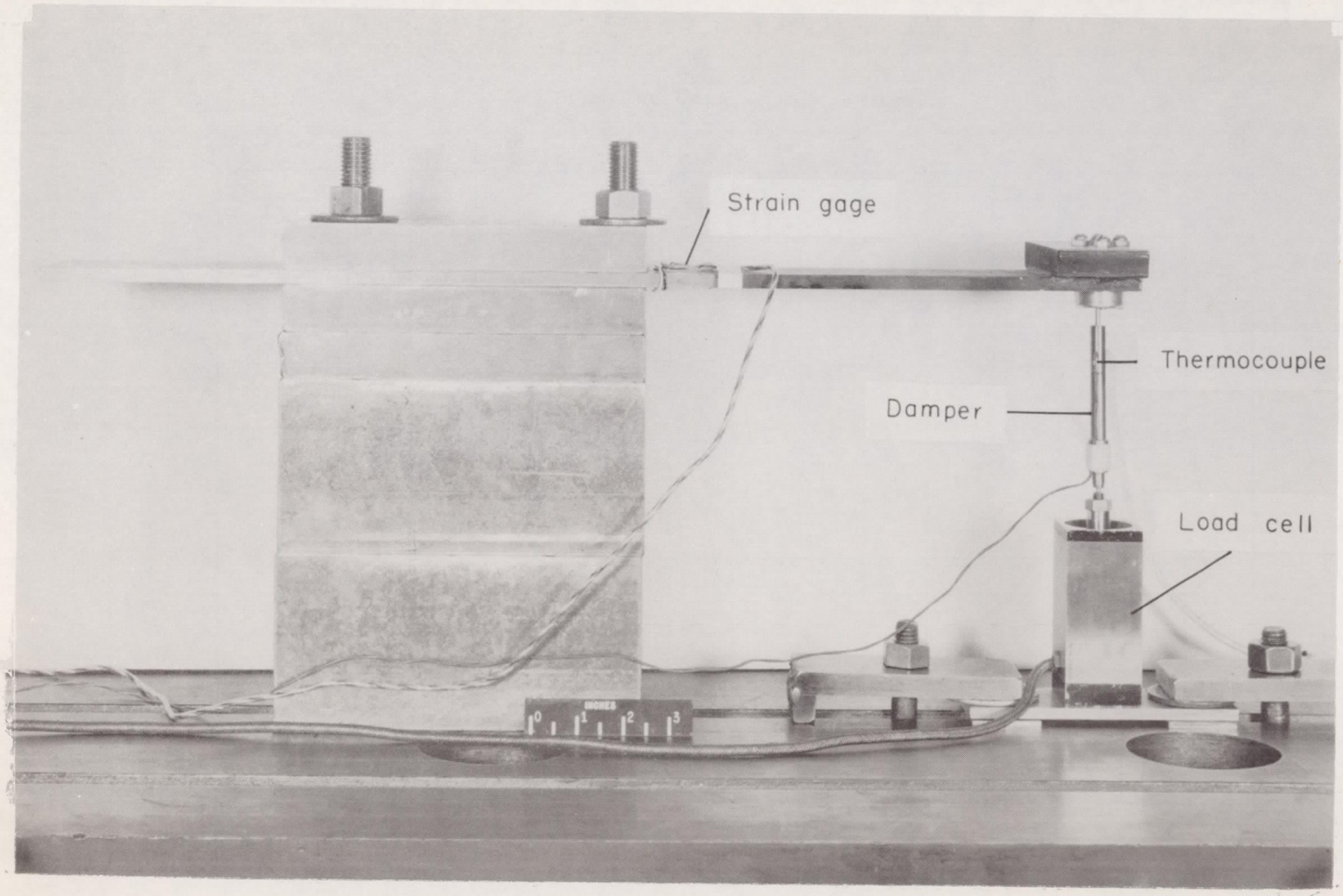

Figure 5.- Beam damper-test device. L-57-1415.1

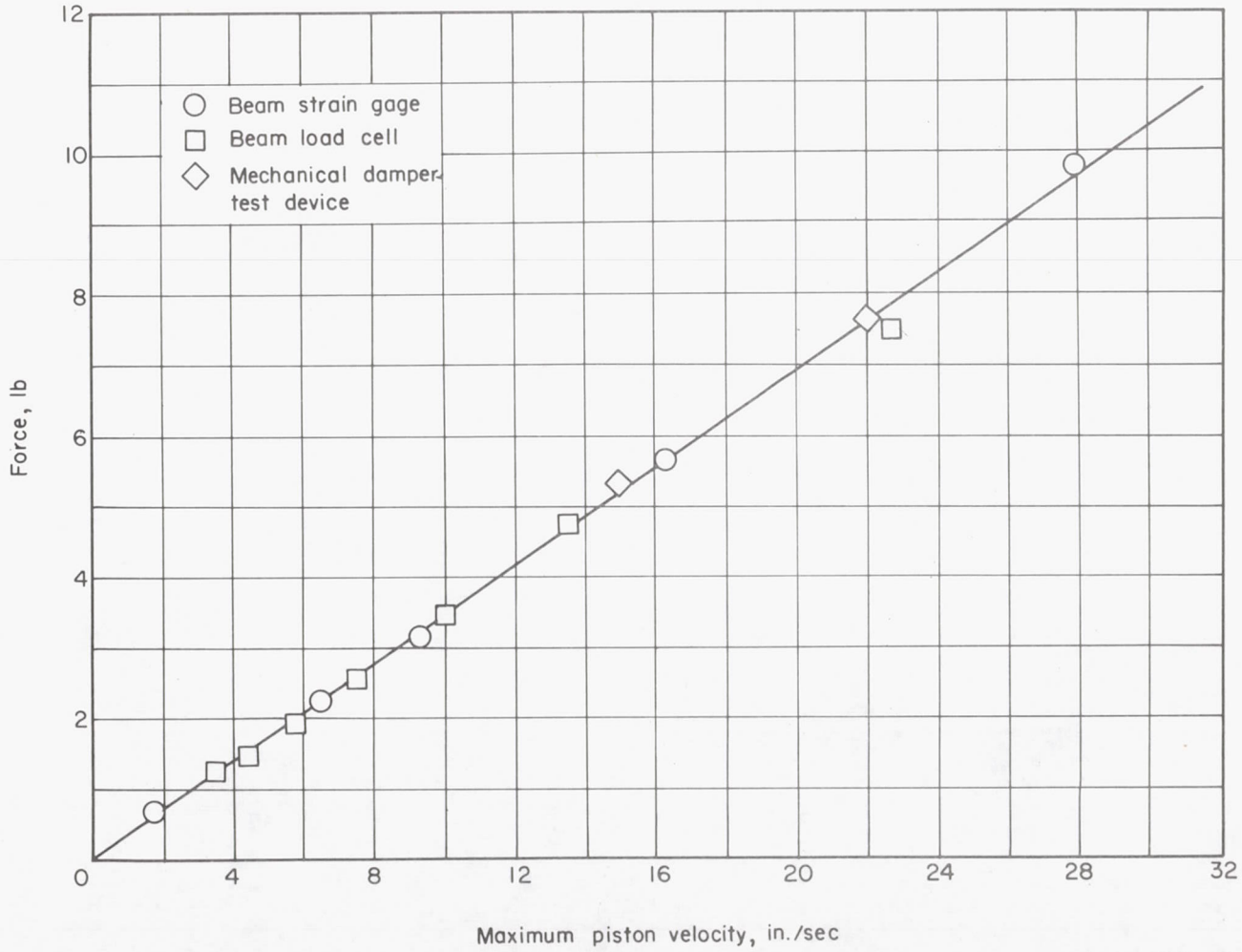

Figure 6.- Comparison of damping force as a function of maximum piston velocity for a fluid-displacement of damper similar to damper A-2 as measured by mechanical damper-test device and by load cell and strain gage of beam damper-test device. Fluid viscosity, 300 Saybolt Universal seconds.

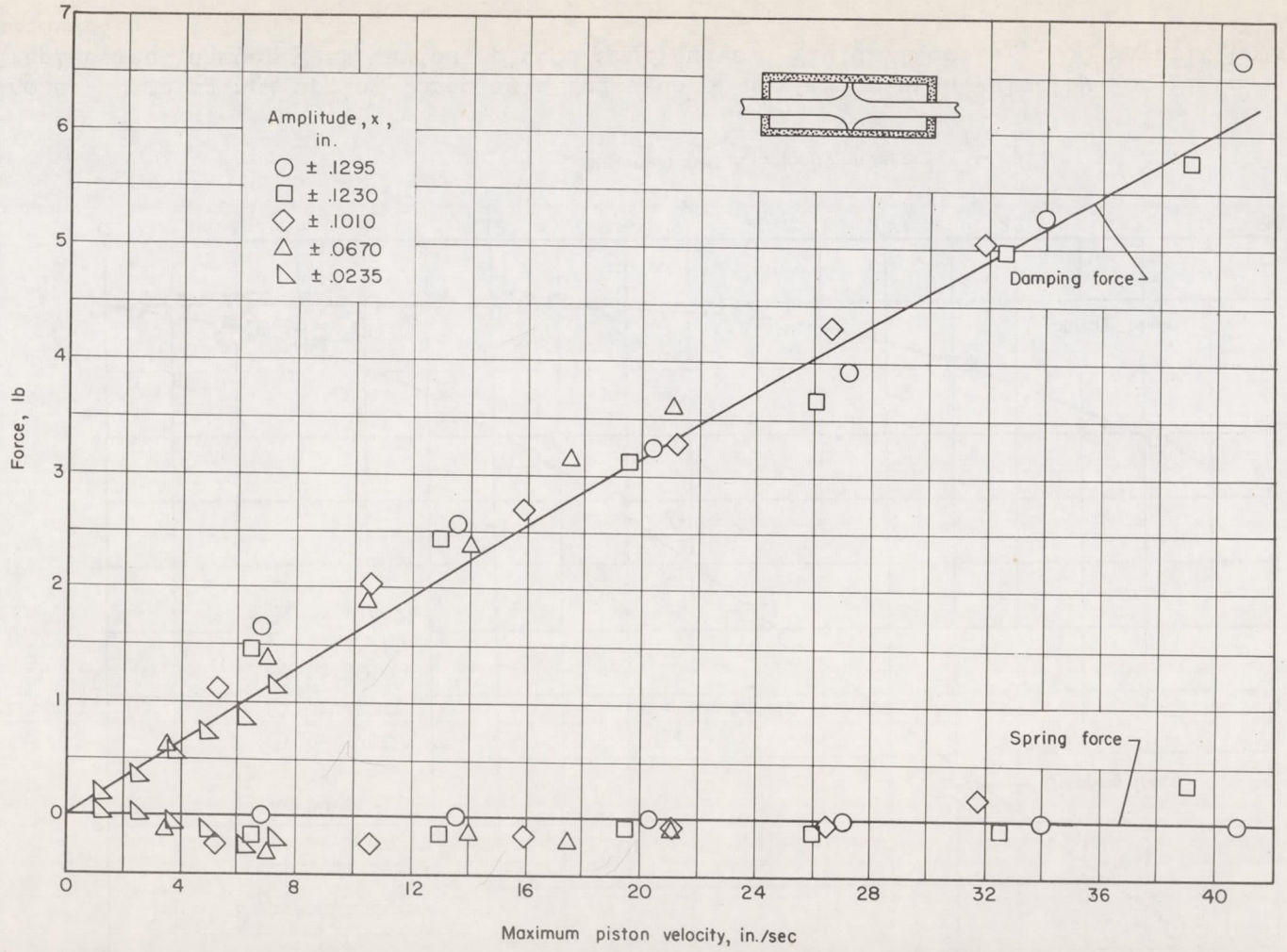

Figure 7.- Damping and spring force as a function of maximum piston velocity for fluid-displacement damper A-2 at various piston amplitudes. Fluid viscosity, 300 Saybolt Universal seconds.

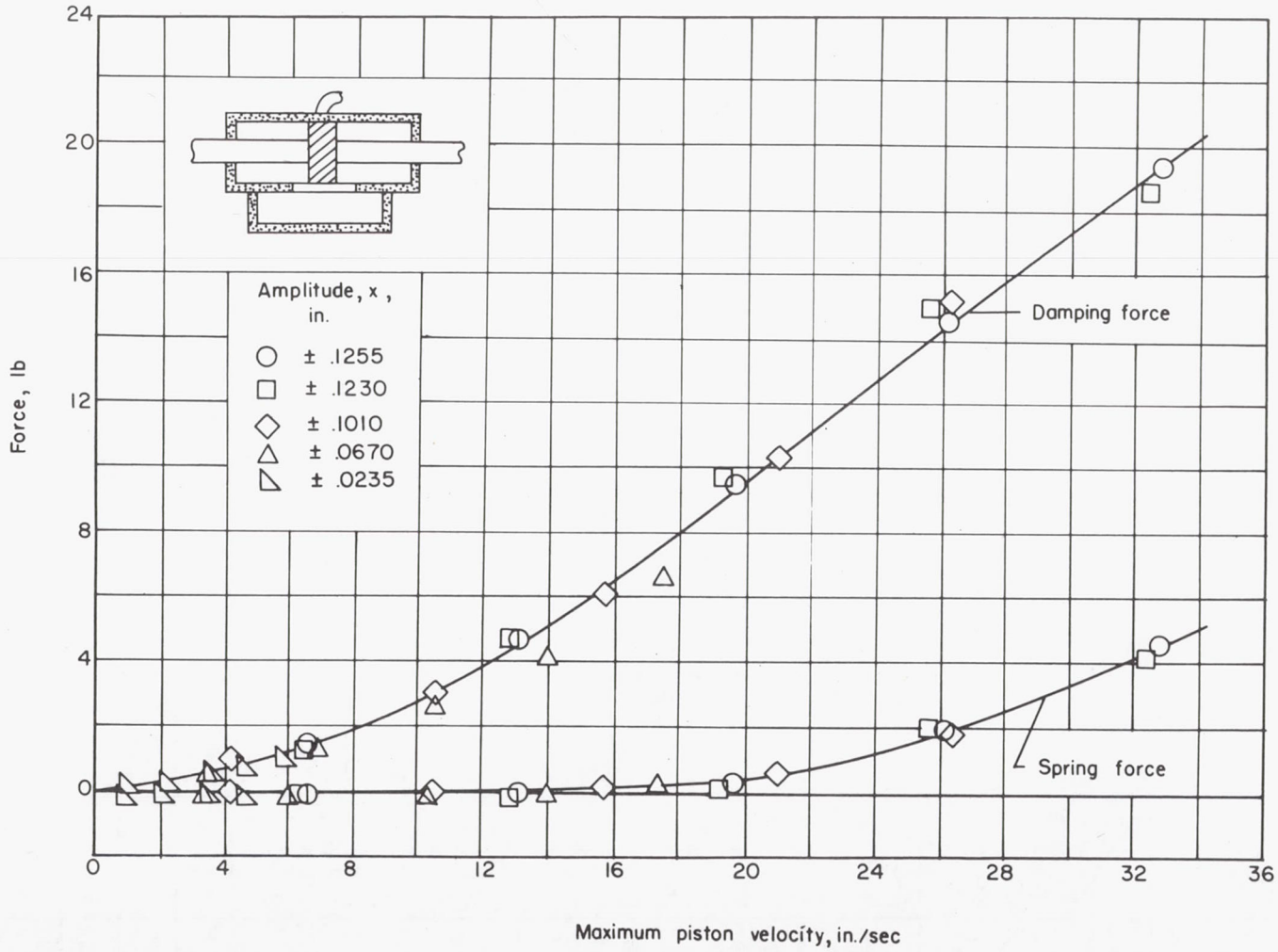

Figure 8.- Damping and spring force as a function of maximum piston velocity for fluid-displacement damper C at various piston amplitudes. Fluid viscosity, 300 Saybolt Universal seconds.

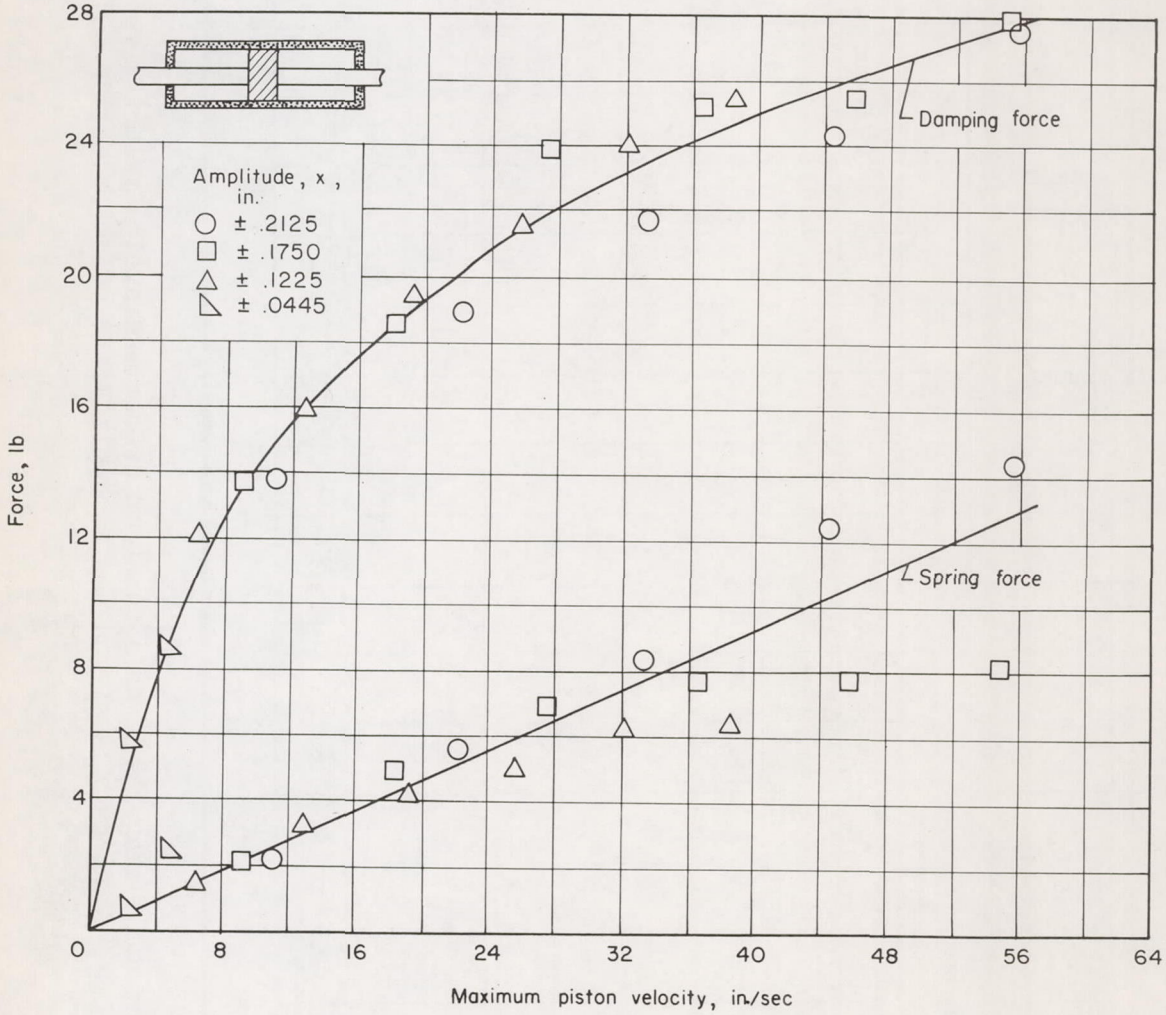

Figure 9.- Damping and spring force as a function of maximum piston velocity for fluid-displacement damper A-1 at various piston amplitudes. Fluid viscosity, 300 Saybolt Universal seconds.

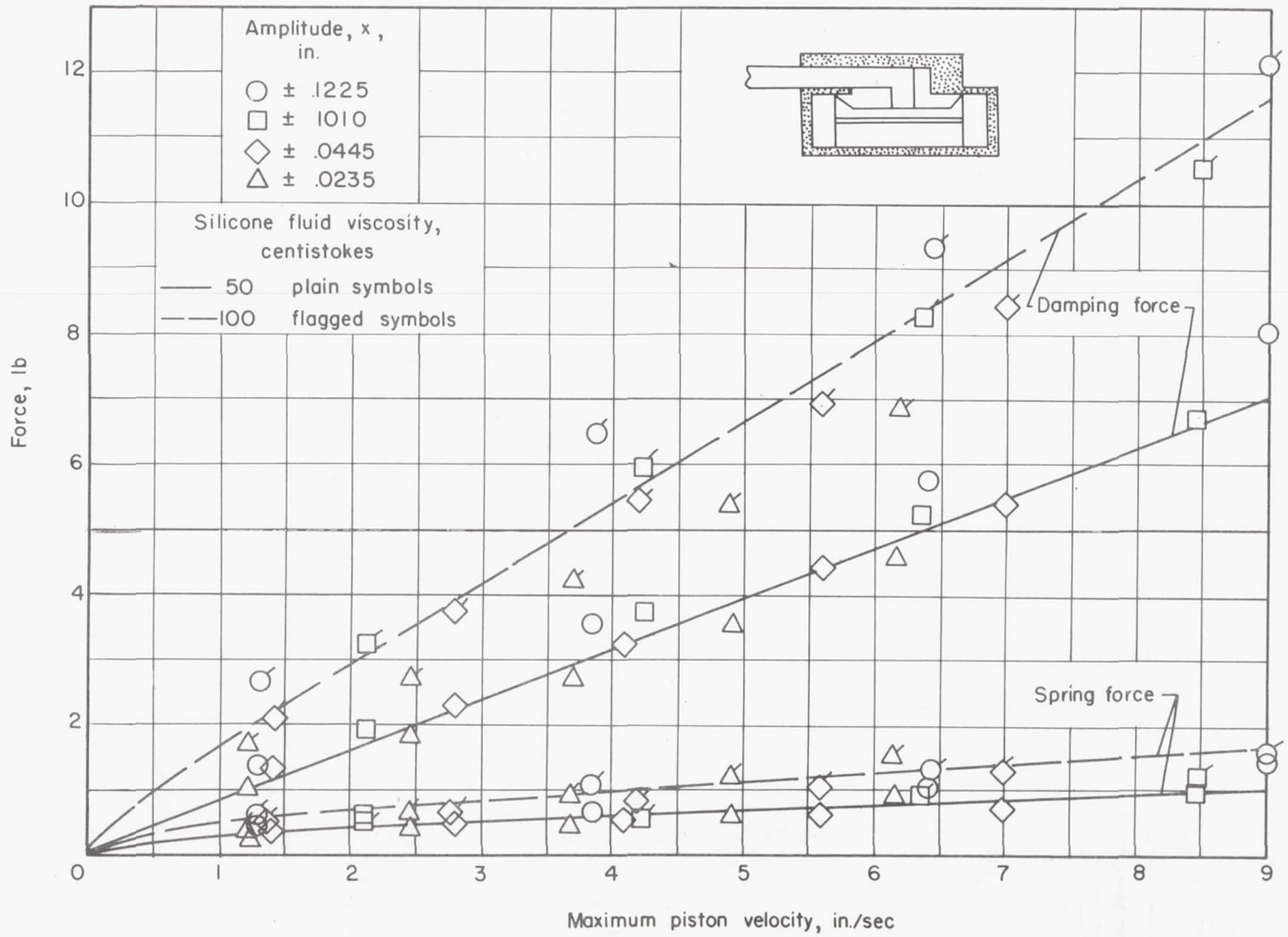

Figure 10.- Damping and spring force as a function of maximum piston velocity for fluid-displacement damper B at various piston amplitudes. Fluid viscosities, 50 and 100 centistokes.

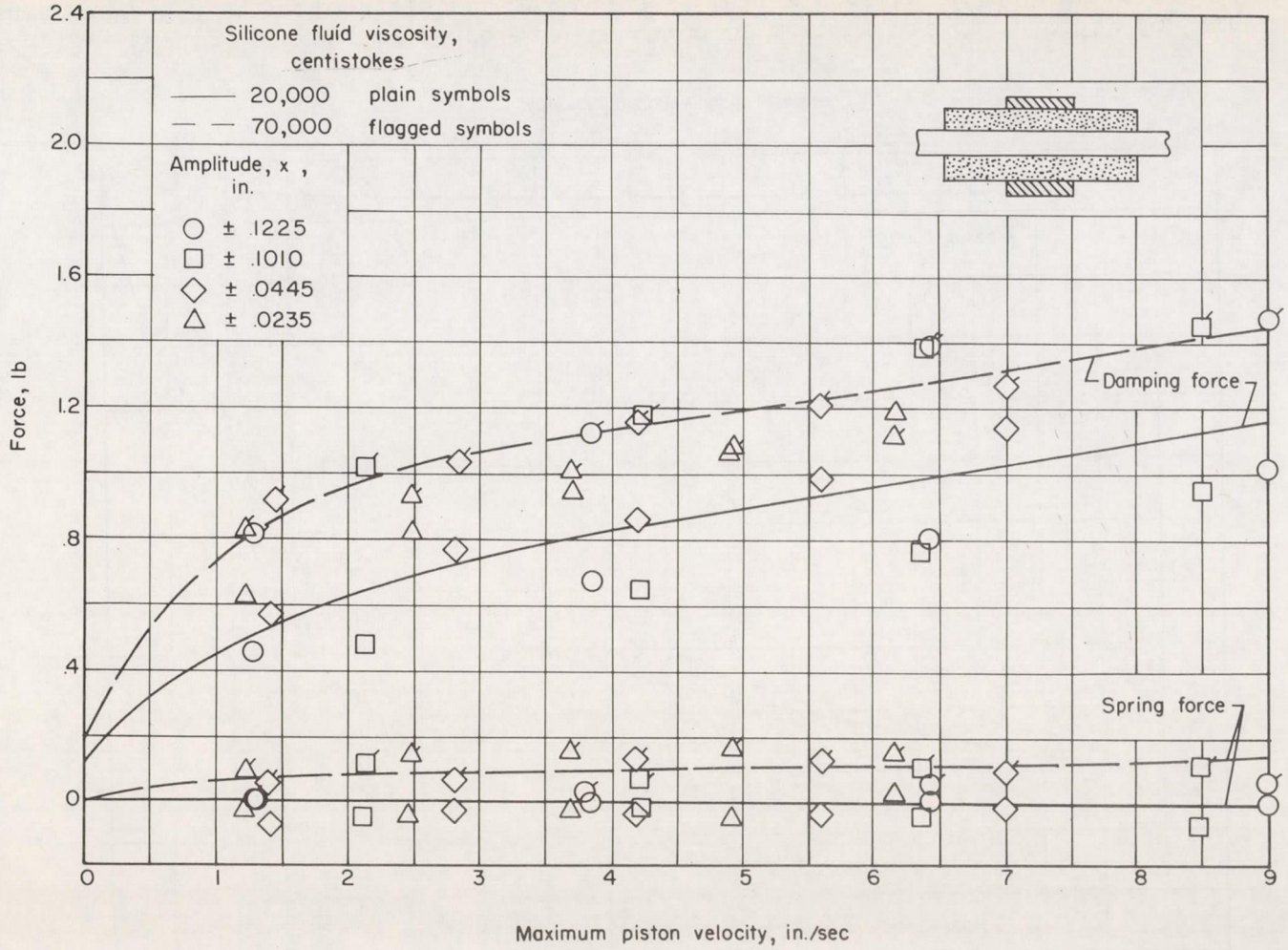

Figure 11.- Damping and spring force as a function of maximum piston velocity for viscous-shear damper F-1 at various piston amplitudes. Fluid viscosities, 20,000 and 70,000 centistokes.

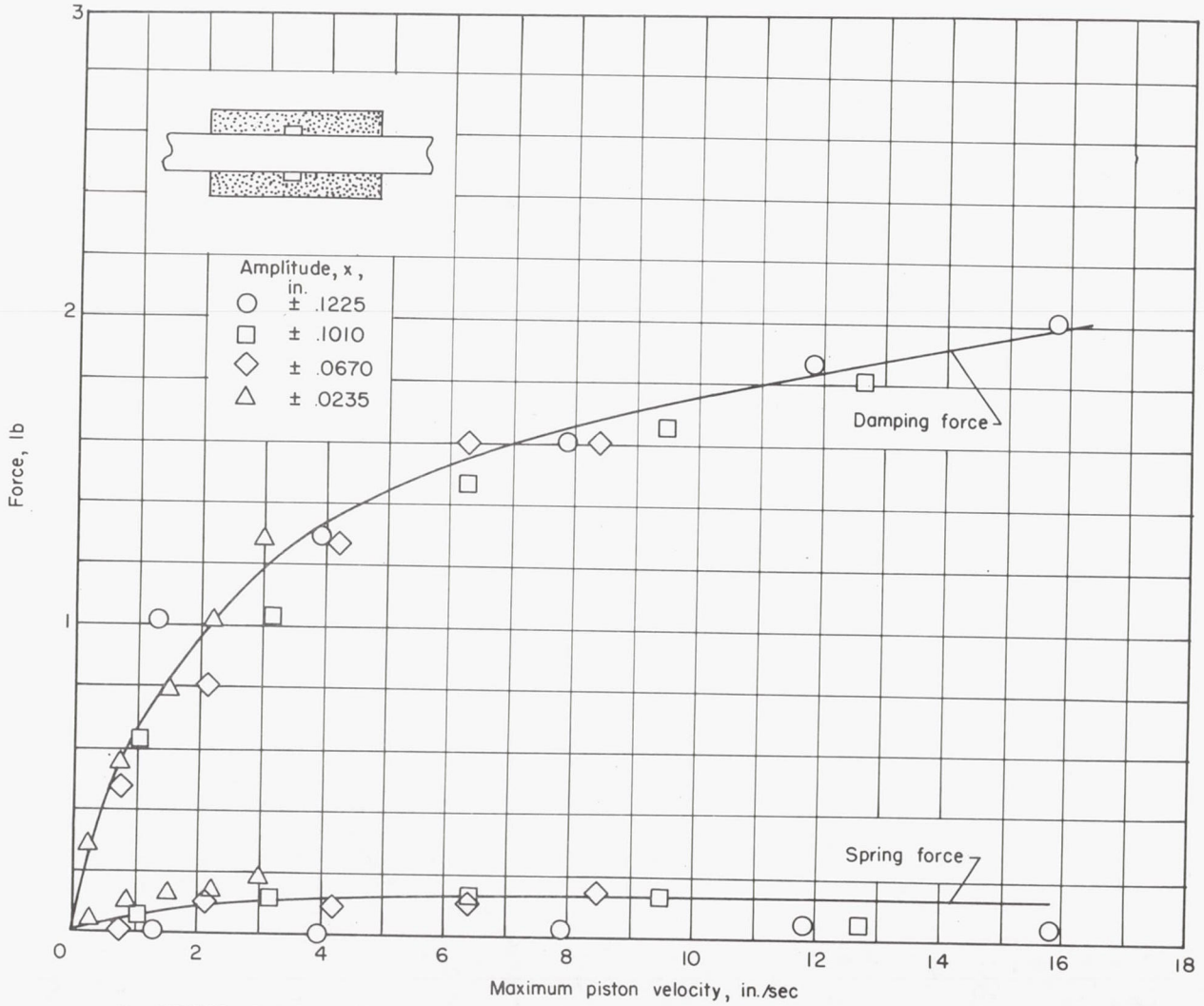

Figure 12.- Damping and spring force as a function of maximum piston velocity for viscous-shear damper J at various piston amplitudes. Fluid viscosity, 70,000 centistokes.

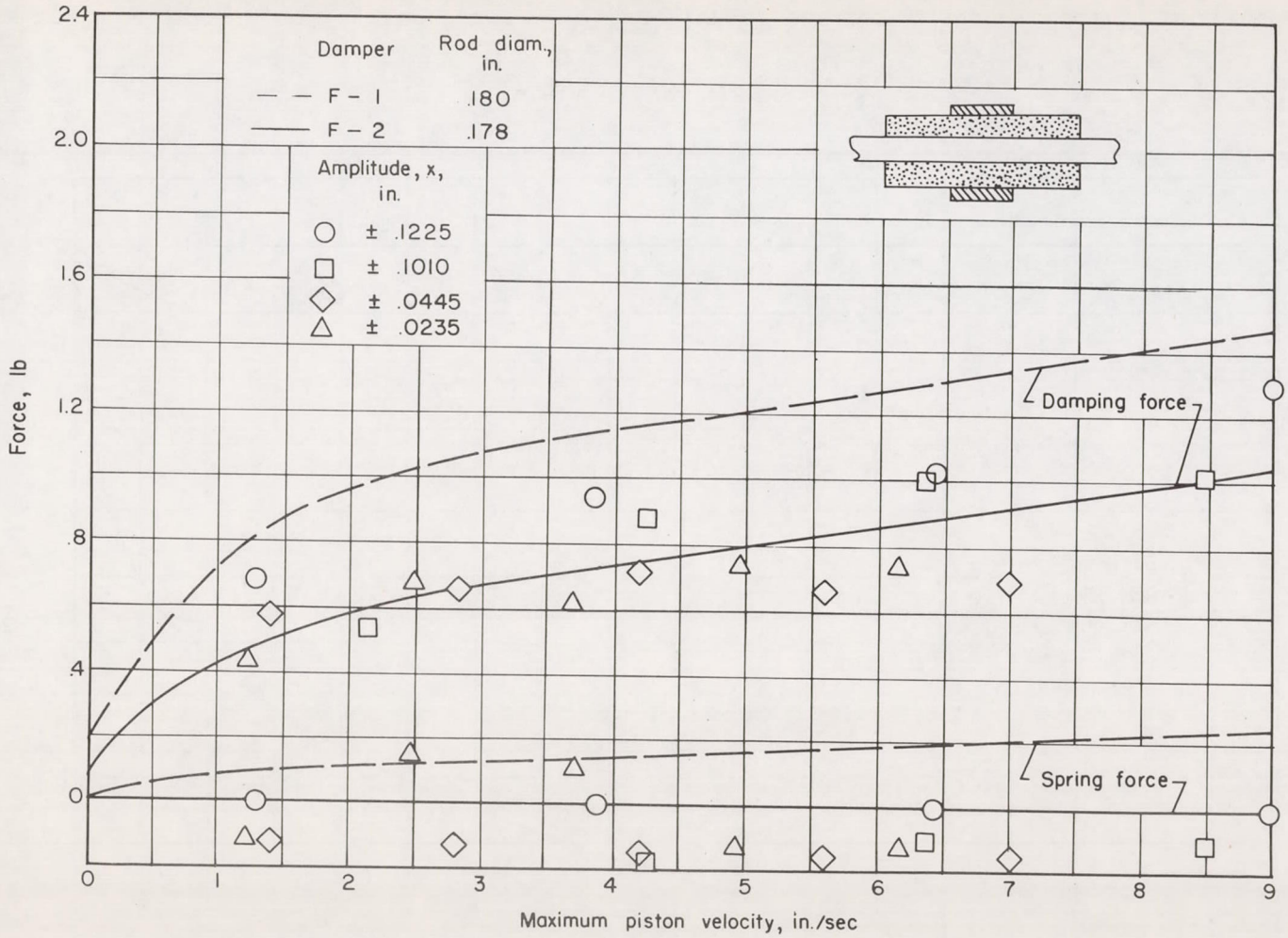

Figure 13.- Damping and spring force as a function of maximum piston velocity for viscous-shear dampers F-1, taken from figure 11, and F-2 at various piston amplitudes. Fluid viscosity, 70,000 centistokes.

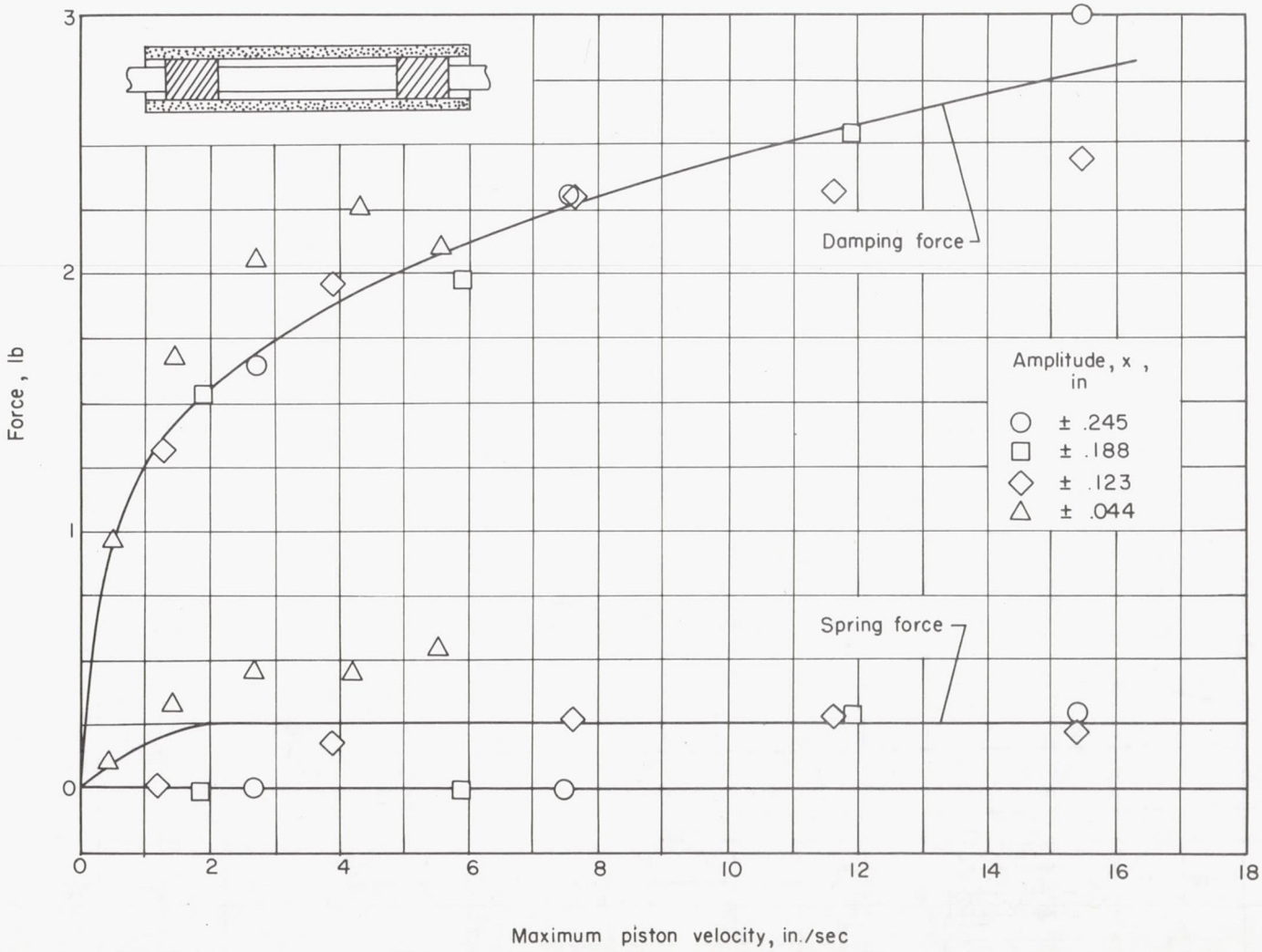

Figure 14.- Damping and spring force as a function of maximum piston velocity for viscous-shear damper H at various piston amplitudes. Fluid viscosity, 70,000 centistokes.

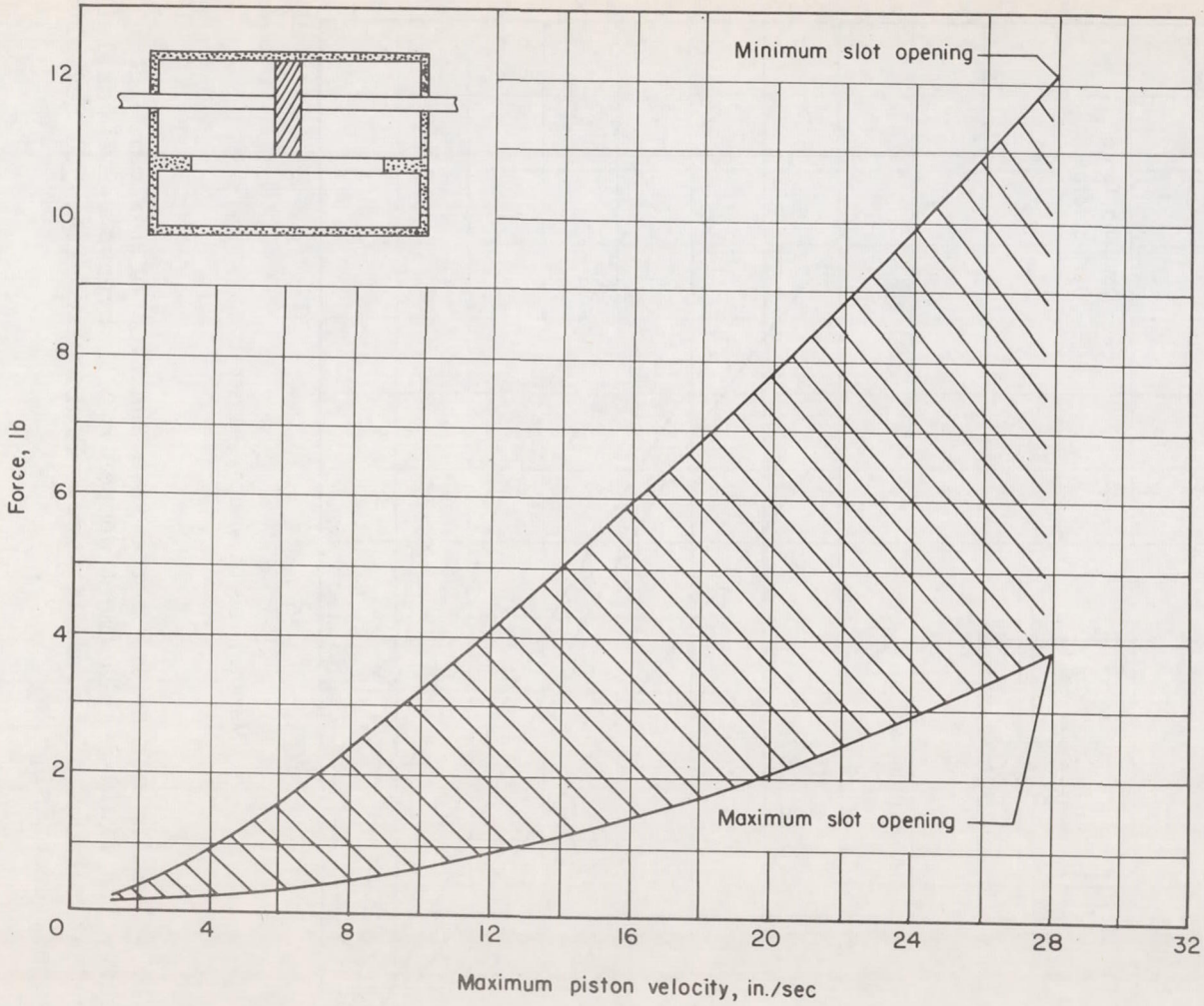

Figure 15.- Range of damping-force values obtainable with fluid-displacement damper D for maximum and minimum slot openings as a function of maximum piston velocity. Fluid viscosity, 300 Saybolt Universal seconds.

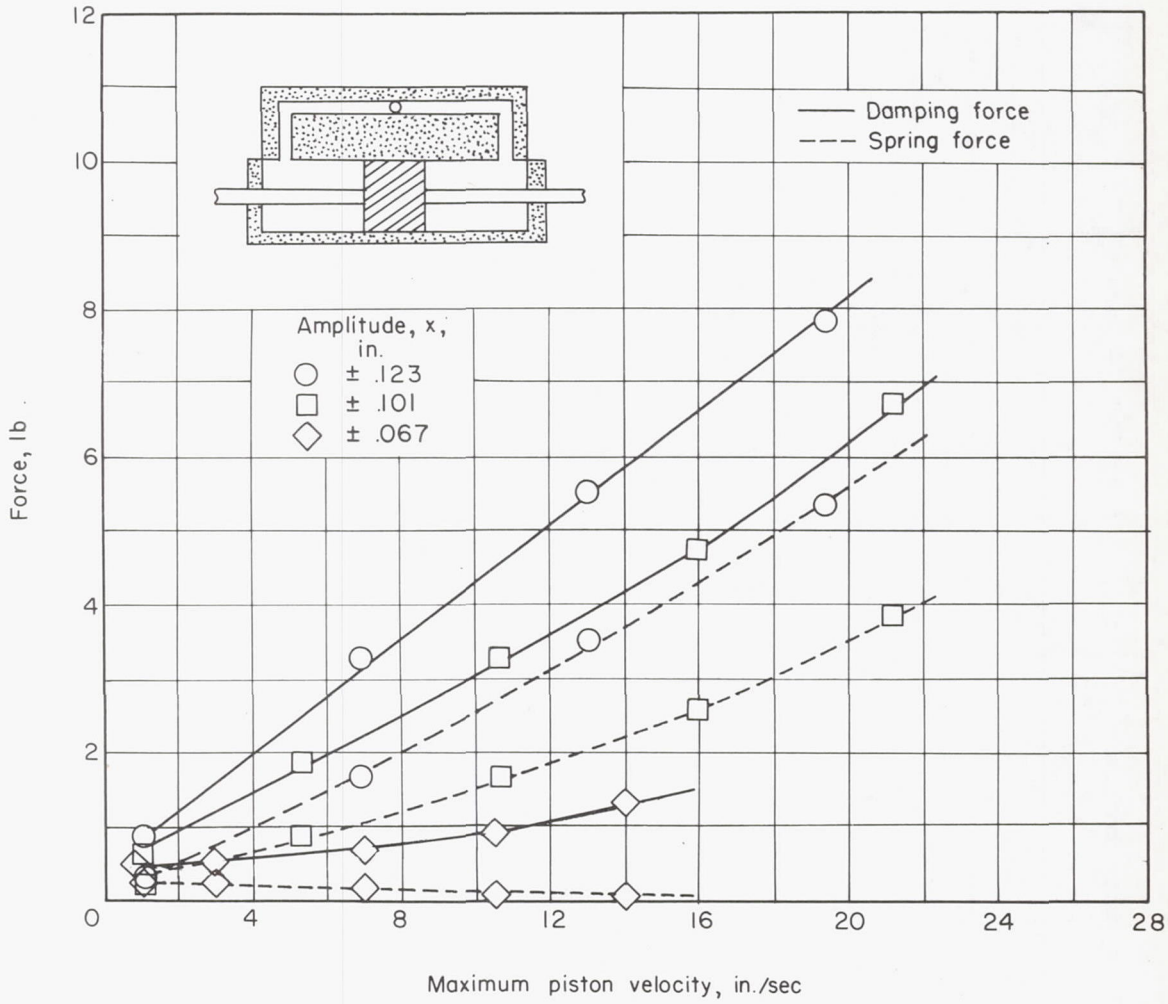

Figure 16.- Damping and spring force as a function of maximum piston velocity for fluid-displacement damper E with bypass valve partially closed at various piston amplitudes. Fluid viscosity, 300 Saybolt Universal seconds.

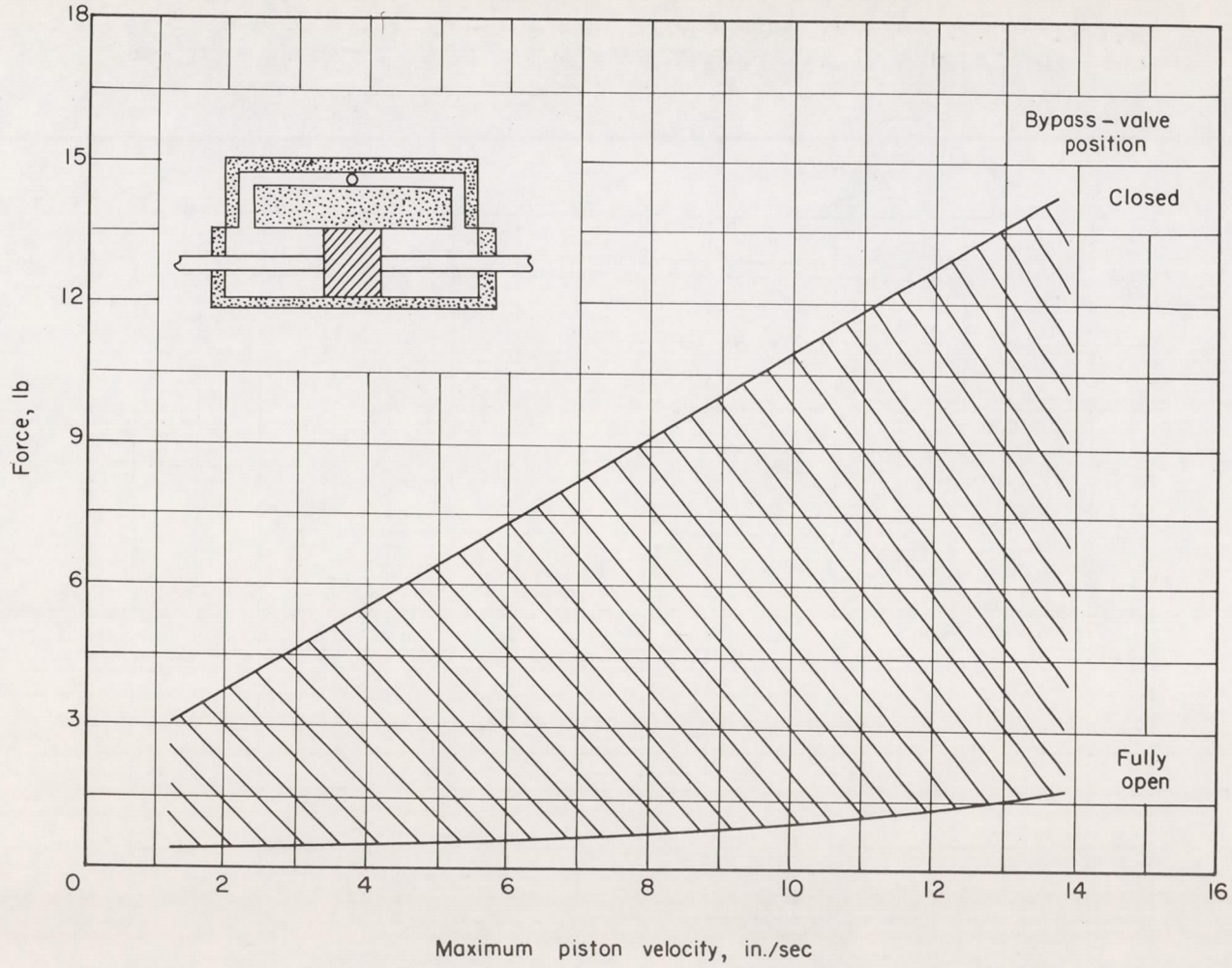

Figure 17.- Range of damping-force values obtainable with damper E with bypass-valve positions ranging from closed to fully open as a function of maximum piston velocity for an amplitude of ±0.123 inch. Fluid viscosity, 300 Saybolt Universal seconds.

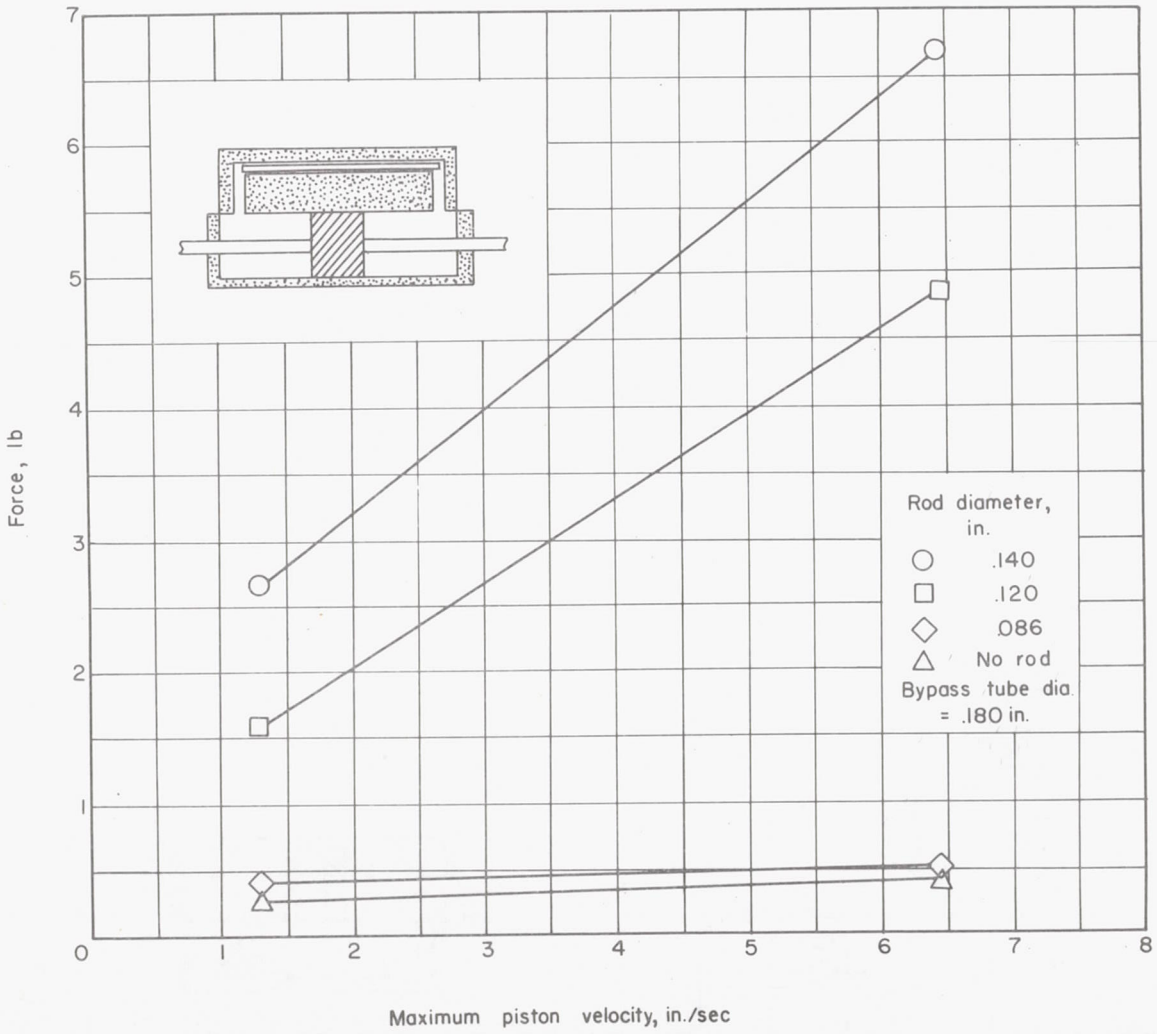

Figure 18.- Range of damping-force values obtainable with fluid-displacement damper E using rods of various diameter in bypass tube as a function of maximum piston velocity for ±0.123-inch amplitude. Fluid viscosity, 300 Saybolt Universal seconds.

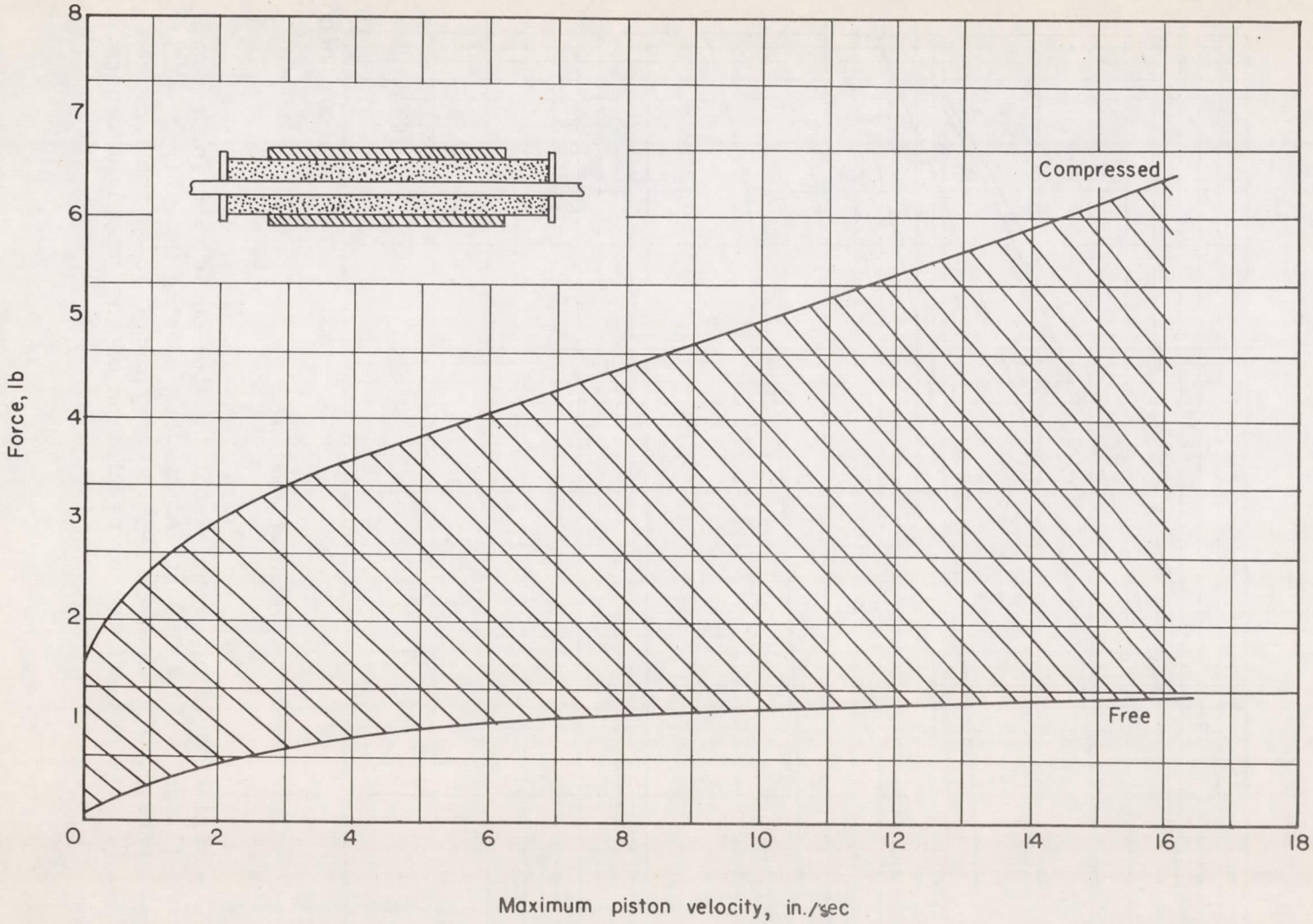

Figure 19.- Range of damping force obtainable with viscous-shear damper G in compressed and free condition as a function of maximum piston velocity. Fluid viscosity, 3,000 centistokes.

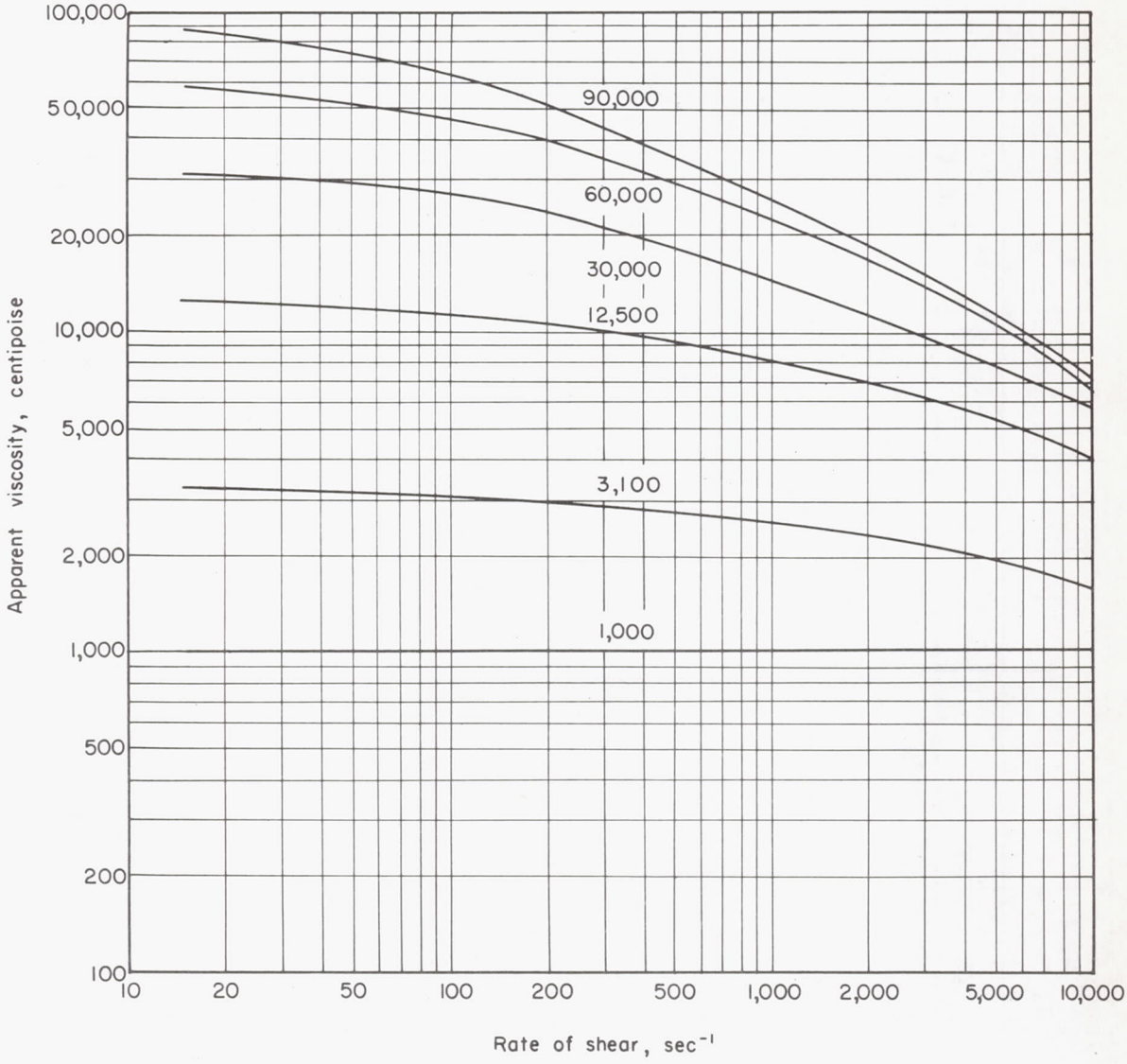

Figure 20.- Variation of apparent viscosity with shear rate for several silicone fluids. (From Industrial and Engineering Chemistry, vol. 42, page 2,457, December 1950. Copyright 1950 by the American Chemical Society and printed by permission of the copyright owners.)

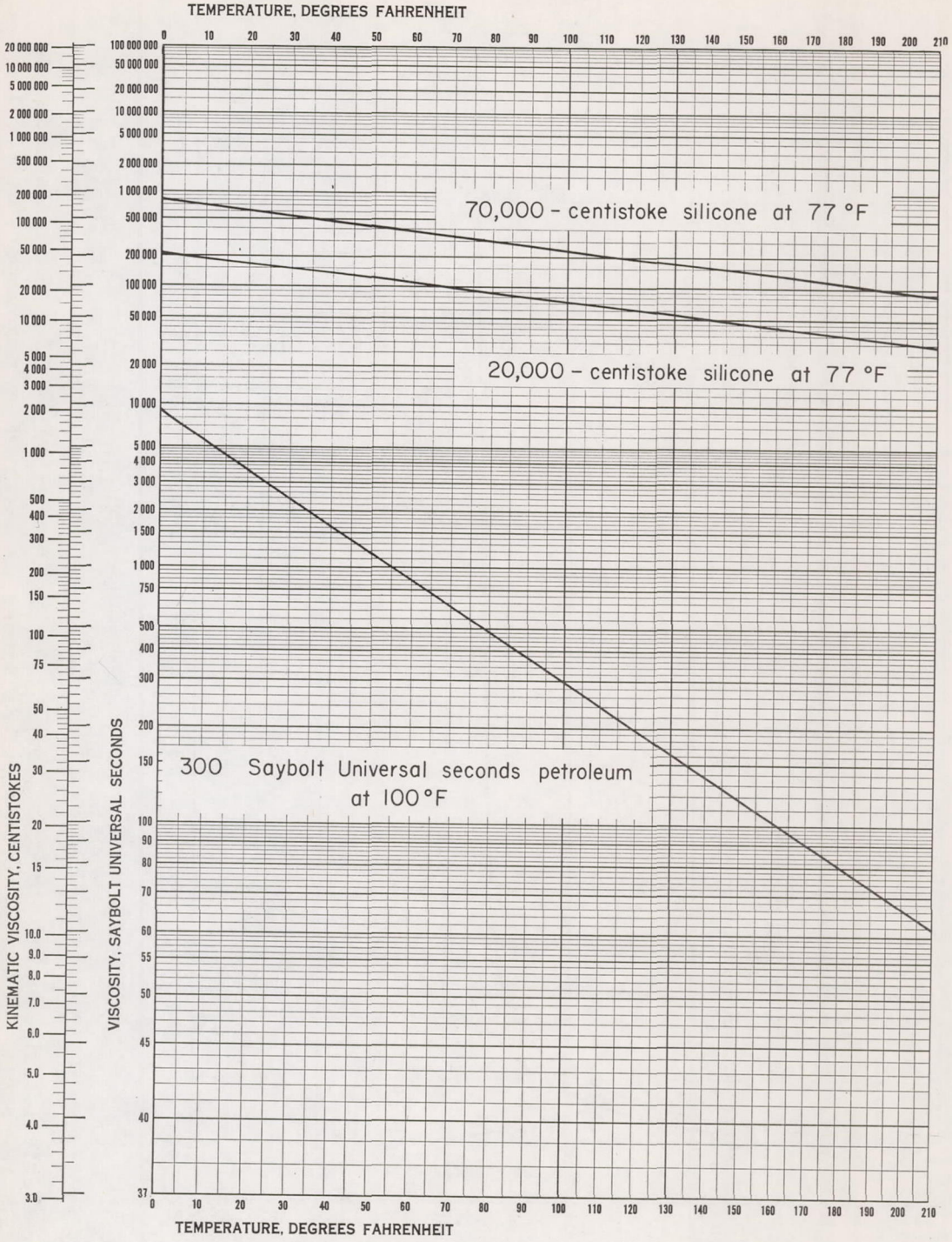

Figure 21.- American Society for Testing Materials standard viscosity-temperature charts for damper fluids employed.

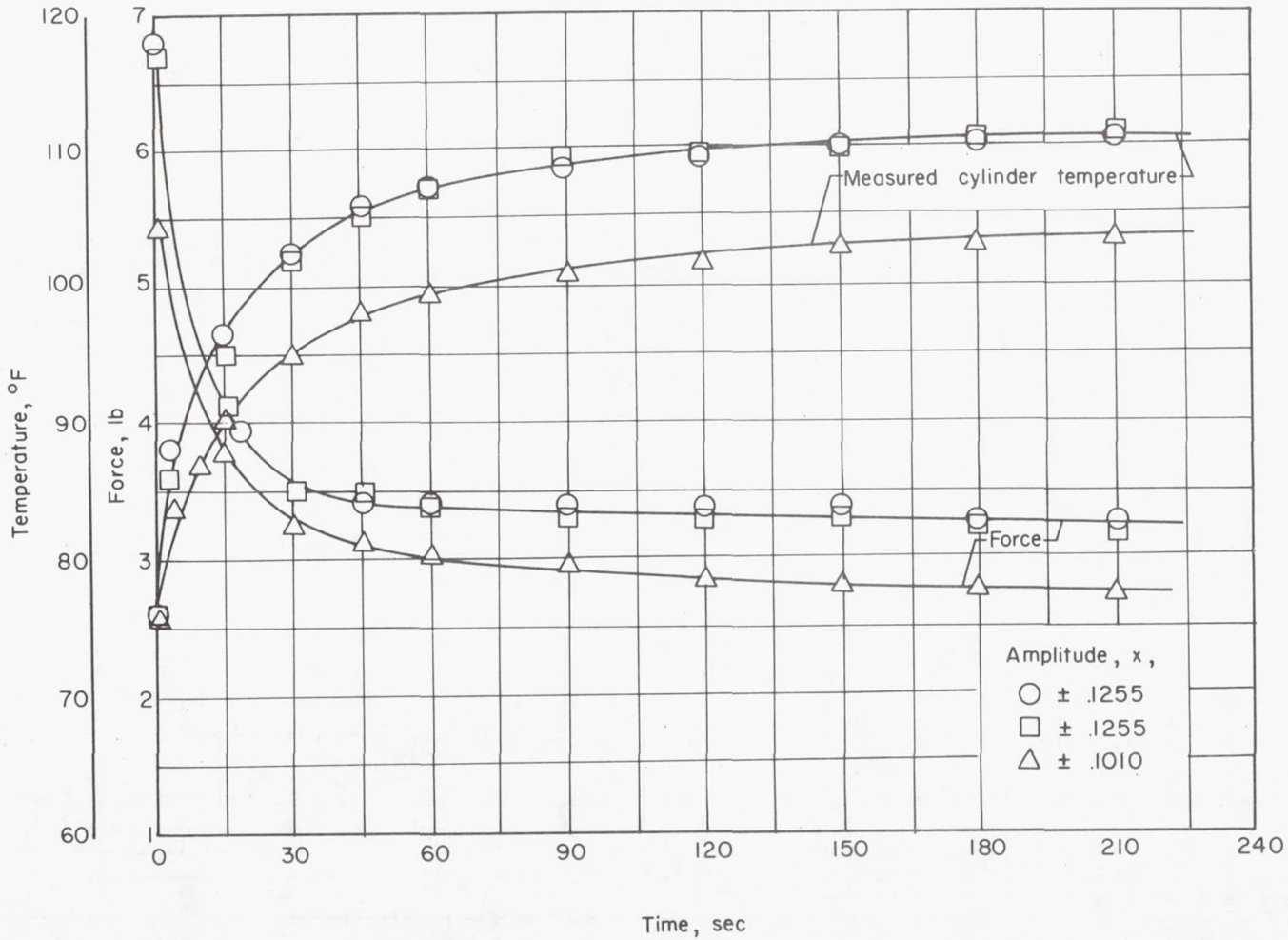

Figure 22.- Variation of damping force and damper temperature with time of a fluid-displacement damper similar to damper A-2 at two piston amplitudes as measured by the damper-test device at a rotational frequency of 25 cps. Fluid viscosity, 300 Saybolt Universal seconds.

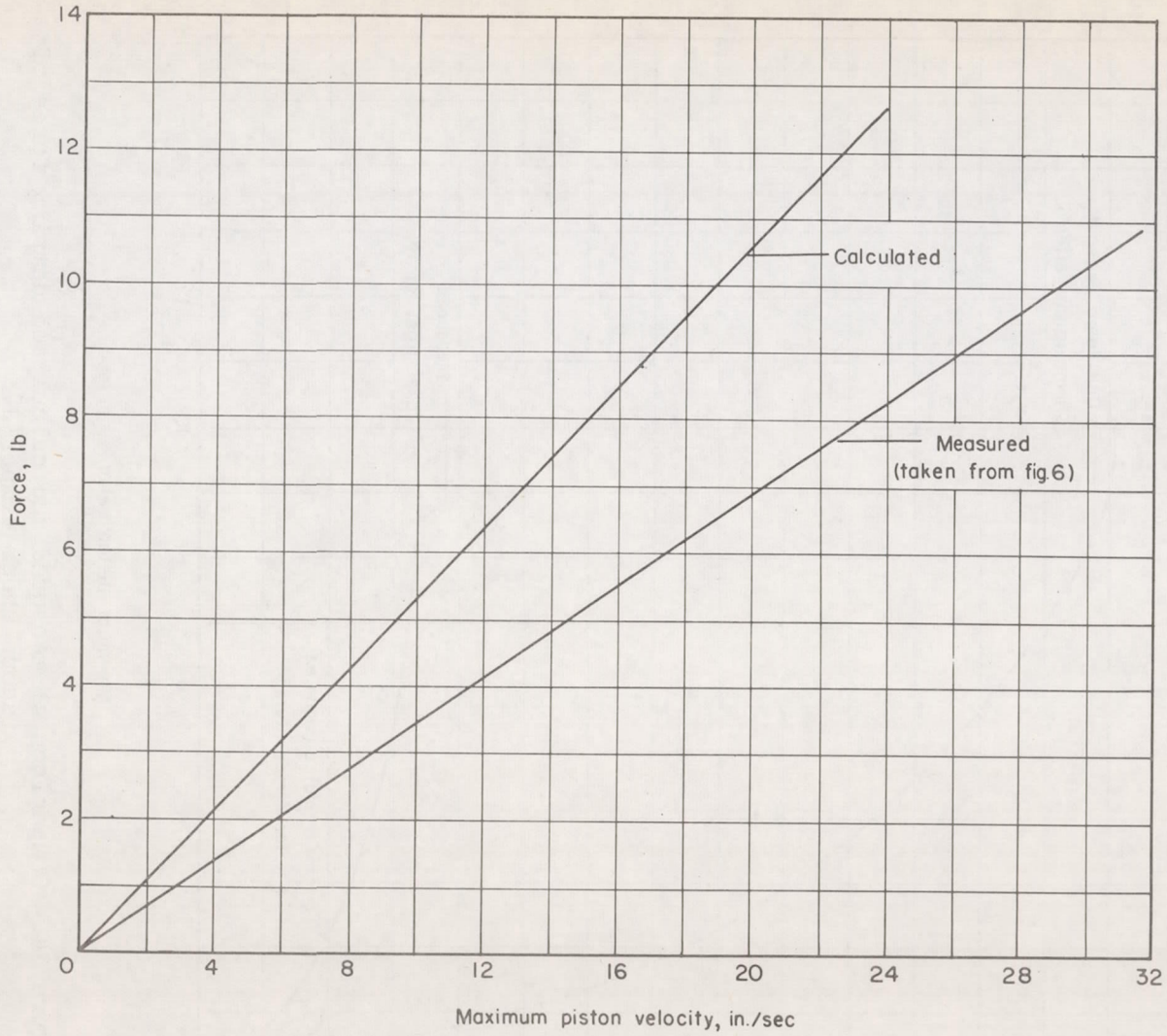

Figure 23.- Comparison of measured and calculated damping force of a fluid-displacement damper similar to damper A-2.

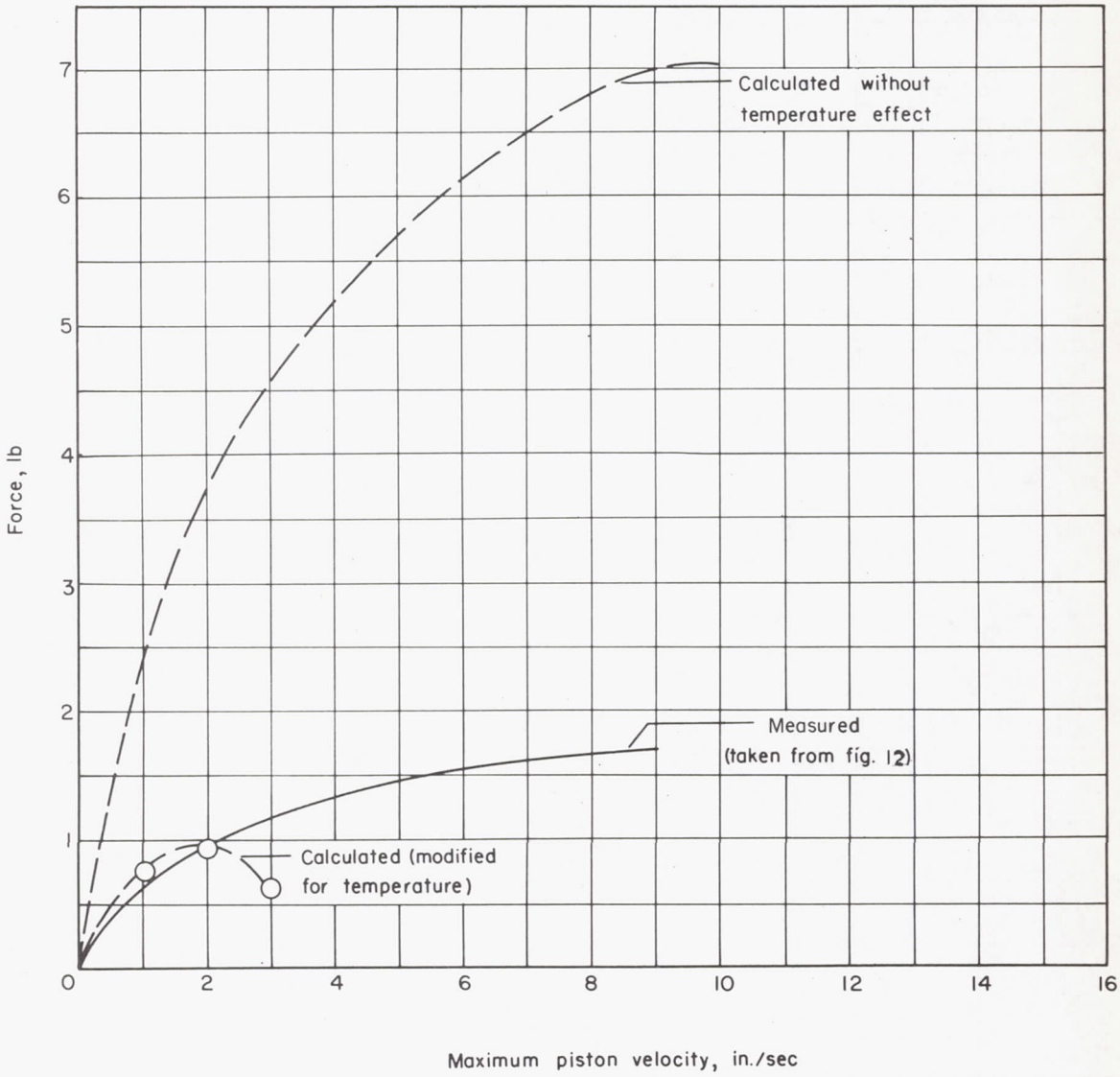

Figure 24.- Comparison of measured and calculated damping force of viscous-shear damper J.

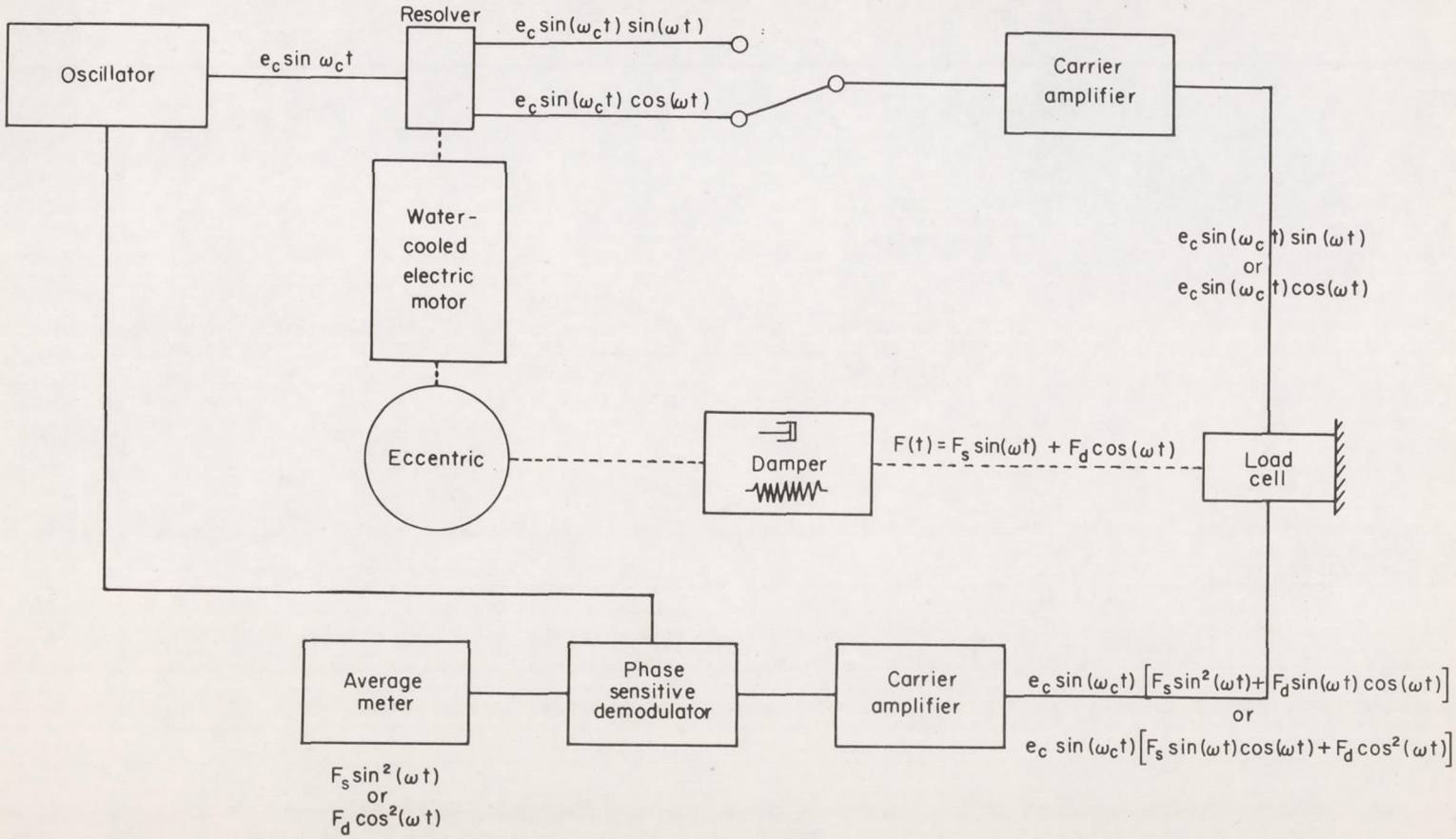

Figure 25.- Block diagram of instrumentation used with the mechanical damper-test device.

NACA - Langley Field, Va.